

# 1 CRISPR-based herd immunity limits 2 phage epidemics in bacterial 3 populations

4 Pavel Payne<sup>1,2\*</sup>, Lukas Geyrhofer<sup>3</sup>, Nicholas H. Barton<sup>2</sup>, Jonathan P. Bollback<sup>1,2\*</sup>

**\*For correspondence:**

[Pavel.Payne@liverpool.ac.uk](mailto:Pavel.Payne@liverpool.ac.uk) (PP);  
[J.P.Bollback@liverpool.ac.uk](mailto:J.P.Bollback@liverpool.ac.uk) (JPB)

5 <sup>1</sup>Institute of Science and Technology Austria, Am Campus 1, Klosterneuburg, Austria;

6 <sup>2</sup>Institute of Integrative Biology, University of Liverpool, Liverpool, UK; <sup>3</sup>Technion – Israel

7 Institute of Technology, Haifa, Israel

8 

---

9 **Abstract** Pathogens are a driving force in evolution, giving rise to a diversity of host immune  
10 defenses. In order for a pathogen to spread in a population a sufficient number of its members  
11 must be susceptible to infection, as resistant individuals can prevent the spread of a pathogen  
12 among susceptible hosts in a process known as herd immunity. While herd immunity has been  
13 extensively studied in vertebrate populations, little is known about its role, if any, in the dynamics  
14 between bacteria and their phage pathogens. Here we explore the dynamics of T7 phage  
15 epidemics in structured and unstructured *Escherichia coli* populations consisting of differing  
16 mixtures of susceptible and resistant individuals harboring CRISPR immunity to the phage. Using  
17 both experiments and mathematical modelling we describe the conditions under which herd  
18 immunity arises in bacterial populations. Notably, the effects of herd immunity depend strongly on  
19 the presence of spatial structure in the population, the bacterial growth rate, and phage replication  
20 rate. The results of our model can apply to other host–pathogen systems to determine the herd  
21 immunity threshold from the relative speed of an epidemic wave in partially resistant populations.  
22 In addition, our findings suggest that herd immunity plays an important role in bacterial  
23 communities, as seen in other host–pathogen systems, allowing for stable coexistence of bacteria  
24 and their phages and the maintenance of polymorphism in bacterial immunity.

25 

---

## 26 Introduction

27 “Herd immunity” has been used in a variety of ways by different authors (see *Fine et al. (2011)*).  
28 Here, we define it as a phenomenon where a fraction of resistant individuals in a population reduces  
29 the probability of transmission of a pathogen among the susceptible individuals. Furthermore, if  
30 the fraction of resistant individuals in a population is sufficiently large the spread of a pathogen is  
31 suppressed. Experimental research into the phenomenon has focused mostly on mammals *Jeltsch*  
32 *et al. (1997)*; *Mariner et al. (2012)*, birds *Boven et al. (2008)*; *Meister et al. (2008)*, and invertebrates  
33 *Konrad et al. (2012)*; *Wang et al. (2013)*. In human populations the principles of herd immunity  
34 were employed to limit epidemics of pathogens through vaccination programs *Fine et al. (2011)*,  
35 which in the case of smallpox lead to its eradication between 1959 and 1977 *Fenner (1993)*.

36 Alongside advances in vaccination programs, the formalization of a general theory of herd  
37 immunity was developed. The theory is based on a central parameter,  $R_0$ , which describes the  
38 fitness of the pathogen, as measured by the number of subsequent cases that arise from one  
39 infected individual in a population (for a historical review of  $R_0$  see *Heesterbeek (2002)*). Thus,  $R_0$   
40 indicates the epidemic spreading potential in a population. Given  $R_0$  the herd immunity threshold

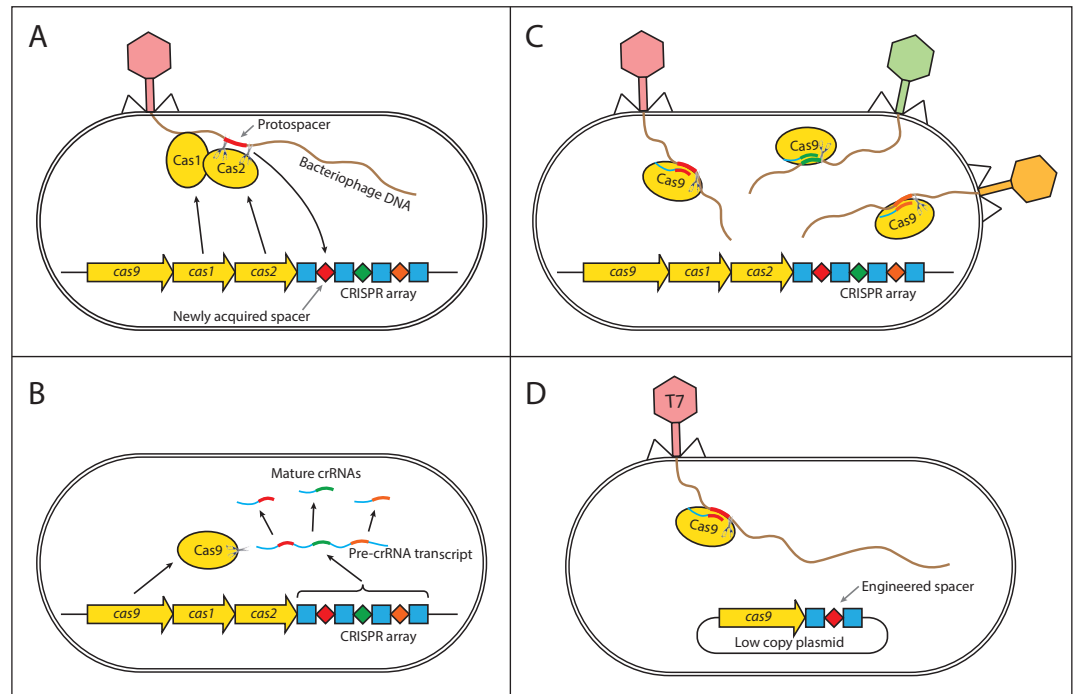


**Figure 1. Mechanism of CRISPR/Cas type II immunity.** The CRISPR/Cas system provides immunity to phages and its main features can be described by three distinct stages. (A) Acquisition. When a cell gets infected by a phage, a protospacer on the invading phage DNA (indicated as a red bar) is recognized by Cas1 and Cas2. The protospacer is cleaved out and ligated to the leader end (proximal to the Cas genes) of the CRISPR array as a newly acquired spacer (red diamond). (B) Processing. The CRISPR array is transcribed as a Pre-crRNA and processed by Cas9 (assisted by RNaseIII and trans-activating RNA, not shown) into mature crRNAs. (C) Interference. Mature crRNAs associate with Cas9 proteins to form interference complexes which are guided by sequence complementarity between the crRNAs and protospacers to cleave invading DNA of phages whose protospacers have been previously incorporated into the CRISPR array. (D) A truncated version of the CRISPR system on a low copy plasmid, which was used in this study lacks *cas1* and *cas2* genes and was engineered to target a protospacer on the T7 phage chromosome to provide *Escherichia coli* cells with immunity to the phage. The susceptible strain contains the same plasmid except the spacer does not target the T7 phage chromosome.

41 is defined as,

$$H = \frac{R_0 - 1}{R_0}, \quad (1)$$

42 which determines the required minimum fraction of resistant individuals needed to halt the spread  
 43 of an epidemic and is effected by the specific details of transmission and the contact rate among  
 44 individuals *Grassly and Fraser (2008)*. Many theoretical studies have addressed the influence of  
 45 some of these details, in particular maternal immunity *Anderson and May (1992)*, age at vaccination  
 46 *Anderson and May (1982)*; *Nokes and Anderson (1988)*, age related or seasonal differences in  
 47 contact rates *Schenzle (1984)*; *Anderson and May (1985)*; *Yorke et al. (1979)*, social structure *Fox*  
 48 *et al. (1971)*, geographic heterogeneity *Anderson and May (1984)*; *Lloyd and May (1996)*; *Real and*  
 49 *Biek (2007)*, and the underlying contact network of individuals *Ferrari et al. (2006)*.

50 Interestingly, little work has focused on the potential role of herd immunity in microbial systems  
 51 which contain a number of immune defense systems and have an abundance of phage pathogens.  
 52 These defenses vary in their potential to provide herd immunity as they target various stages of the  
 53 phage life cycle, from adsorption to replication and lysis. Early defense mechanisms include the  
 54 prevention of phage adsorption by blocking of phage receptors *Nordström and Forsgren (1974)*,  
 55 production of an extracellular matrix *Hammad (1998)*; *Sutherland et al. (2004)*, or the excretion of  
 56 competitive inhibitors *Destoumieux-Garçon et al. (2005)*. Alongside these bacteria have evolved  
 57 innate immune systems that target phage genomes for destruction. These include host restriction-

58 modification systems (RMS) *Blumenthal and Cheng (2002)*, argonaute-based RNAi-like systems  
59 *Swarts et al. (2014)*, and bacteriophage-exclusion (BREX) systems *Goldfarb et al. (2015)*. In addition  
60 to innate systems, bacteria have evolved an adaptive immune system called CRISPR-Cas (clustered  
61 regularly interspaced short palindromic repeat) *Sorek et al. (2013)*. In order for any of these immune  
62 systems to provide herd immunity, they must prevent further spread of the pathogen, i.e., provide  
63 a 'sink' for the infectious particles reducing the average number of successful additional infections  
64 below one. Unlike the early defense mechanisms that may simply prevent an infection but not the  
65 further reproduction of infectious particles, the RMS, BREX, argonaute-based RNAi-like, and the  
66 CRISPR-Cas systems degrade foreign phage DNA after it is injected into the cell, and thus continue  
67 to remove phage particles from the environment, which increases their potential to provide herd  
68 immunity. Among these the CRISPR-Cas system is unique in that it is adaptive allowing cells to  
69 acquire immunity upon infection (see Fig 1A, B, and C), which can lead to polymorphism in immunity  
70 and give rise to herd immunity.

71 In addition to immune system-specific factors, the reproductive rate of phage depends strongly  
72 on the physiology of the host bacterium *Hadas et al. (1997)*, and the underlying effective contact  
73 network which may vary greatly in bacterial populations depending on the details of their habitat.  
74 Thus, herd immunity will be influenced by the physiological state of the bacteria and the mobility  
75 of the phage in the environment through passive diffusion and movement of infected individuals.  
76 Taken together these details call into question the applicability of the traditional models of herd  
77 immunity from vertebrates to phage-bacterial systems. Thus, experimental investigation and  
78 further development of extended models that take into account the specifics of microbial systems  
79 are required.

80 To investigate under which conditions herd immunity may arise in bacterial populations, we  
81 constructed an experimental system consisting of T7 phage and bacterial strains susceptible and  
82 resistant to it. Our experimental system can be characterized by the following features. First,  
83 we used two strains of *Escherichia coli*, one with an engineered CRISPR-based immunity to the T7  
84 phage, and the other lacking it (Fig 1D). Second, we examined the dynamics of the phage spread in  
85 different environments – spatially structured and without structure. Furthermore, we developed  
86 and analyzed a spatially explicit model of our experimental system to determine the biologically  
87 relevant parameters necessary for bacterial populations to exhibit herd immunity.

## 88 Results

### 89 Properties of resistant individuals

90 We engineered a resistant *E. coli* strain by introducing the CRISPR-Cas Type II system from *Streptococ-*  
91 *cus pyogenes* with a spacer targeting the T7 phage genome (see Material and Methods). We further  
92 characterized the ability of the system to confer resistance to the phage. We find a significant level  
93 of resistance as measured by the probability of cell burst when exposed to T7 (Fig 2A). However,  
94 resistance is not fully penetrant as approximately 1 in 1000 resistant cells succumb to infection. In  
95 addition, we observe that as phage load increases (multiplicity of infection, MOI) the probability  
96 that a cell bursts increases (Fig 2A). In order to determine the herd immunity threshold in our  
97 experimental system, we constructed the resistant strain such that upon infection the cell growth  
98 is halted, yet the cell still adsorbs and degrades phages (Fig 2B,C). This feature is important as it  
99 prevents the action of frequency dependent selection which in naturally growing populations will  
100 favor the resistant strain until its frequency reaches the herd immunity threshold. Thus, in our  
101 system if the frequency of the resistant strain is below the herd immunity threshold, the resistant  
102 cells remain below the threshold and are unable to stop the epidemic and the whole population  
103 collapses. In contrast, if the frequency of resistant individuals in the population is above the herd  
104 immunity threshold, the resistant individuals provide complete herd immunity and the population  
105 survives. These properties allow us to quantify the expanding epidemic in both liquid media and on  
106 bacterial lawns (without and with spatial structure, respectively) using high throughput techniques.

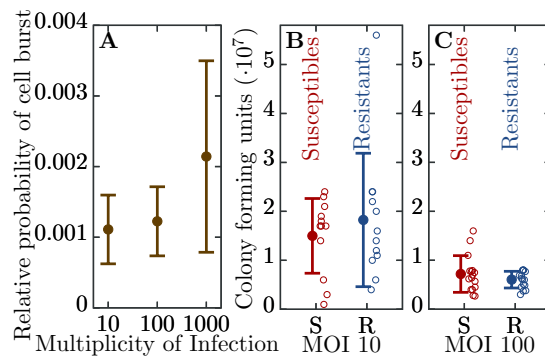


**Figure 2. Efficiency of bacterial resistance.** (A) The probability that a resistant cell bursts, relative to a susceptible cell, at three different initial multiplicities of infection (MOI). The probability that a resistant cell bursts at MOI 1000 is significantly higher than at MOI 10 ( $p = 0.019$ ,  $t_{4,0.05} = 3.031$ ) or at MOI 100 ( $p = 0.022$ ,  $t_{5,0.05} = 2.674$ ). The error bars show the standard deviations from the mean. Note that this measure is not a widely used ‘efficiency of plating’ but it determines the probability of burst of single resistant cells (see Materials and Methods for details). (B) The number of colony forming units (CFUs) post phage challenge (see Materials and Methods). The mean number of CFUs after the bacterial cultures were exposed to the phage is not significantly different between susceptible and resistant strains at MOI 10 ( $p = 0.239$ ,  $t_{22,0.05} = 0.721$ ) and (C) at MOI 100 ( $p = 0.27$ ,  $t_{30,0.05} = 1.124$ ), indicating that the resistant cells’ growth is halted after the cells are infected by a phage. The error bars show the standard deviations from the mean. There were no detectable CFUs in either susceptible or resistant cell cultures at MOI 1000. It should be noted that the indicated MOI values do not correspond to the average number of phages that adsorb to cells in the experiments. For MOI 10 we estimated the mean number of phages per cell as 0.229 and for MOI 100 as 0.988 (see Materials and Methods for details). It was impossible to determine the mean for MOI 1000 as there were no detectable CFUs under such conditions.

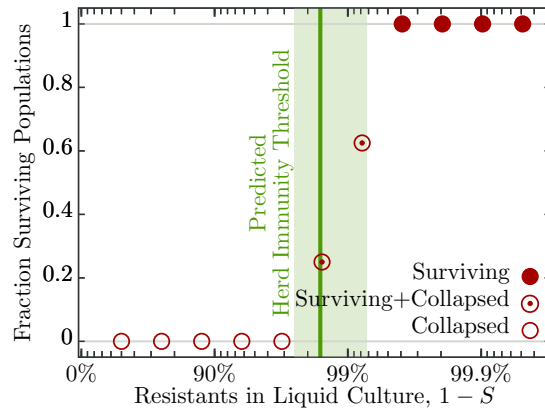


**Figure 3. Fraction of surviving populations at 18 h post phage infection.** Bacterial populations consisting of various fractions of resistant to susceptible individuals infected with  $\approx 50$  phages, corresponding to a multiplicity of infection (MOI) of  $\approx 10^{-4}$ , to resemble an epidemic initiated by the burst size from one infected individual (see Table 2 for burst size estimates). Each population phage challenge is replicated 16 times. The solid dark green line shows the model prediction, Eqn. (4), for the herd immunity threshold ( $H$ ), given latent period ( $\lambda$ ), bacterial growth rate ( $\alpha$ ), and phage burst size ( $\beta$ ). Shaded area indicates  $\pm 1$  standard deviation.

107 Specifically, it allows us to control for the complex dynamics of the system arising from frequency  
 108 dependent selection and simultaneous changes in the physiological states of the cells (growth rates  
 109 depending on the nutrient concentrations) and phage (burst size, latent period depending on the  
 110 cells’ physiology).

### 111 Herd immunity in populations without spatial structure

112 To understand the influence of spatial population structure, or lack thereof, we first measured the  
 113 probability of population survival (i.e., whether the cultures are cleared or not) in well mixed liquid  
 114 environments (no spatial structure) consisting of differing proportions of resistant to susceptible

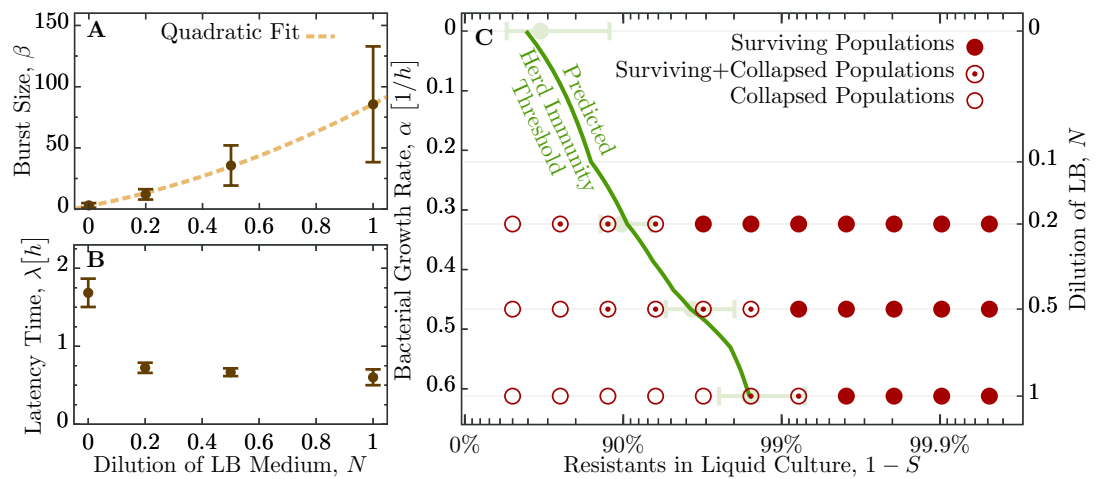


**Figure 4. Herd immunity threshold in liquid culture as a function of bacterial growth.** (A) Phage burst size ( $\beta$ ) change as a function of nutrient concentrations. Brown dashed line shows a numerical quadratic fit to the observed values of  $\beta$ . (B) Latent period ( $\lambda$ ) increase across the range of nutrient concentrations. Values for  $\beta$  and  $\lambda$  are given in Table 2. (C) Population survival analysis upon phage challenge as a function of the fraction of resistant cells and the intrinsic growth rate (nutrient availability,  $N$ ). The empty circles, circled dots, and filled circles represent the outcomes of 18 replicates done in 3 independent batches, as indicated in the legend. The green line shows the model predicted herd immunity threshold given by Eqn. (5), using a quadratic fit for  $\beta/\lambda$  and inverting the Monod kinetics of bacterial growth (see Fig 6B) numerically. Light green error-bars are estimates from Eqn. (5) using actual experimental results for growth parameters.

115 individuals and T7 phage. When the percentage of resistant individuals is in excess of 99.6% all  
 116 16 replicate populations survive a phage epidemic (i.e., show no detectable difference in growth  
 117 profiles to the phage free controls; Fig 3). Populations with 99.2% and 98.4% resistant individuals  
 118 show intermediate probabilities of survival – 10 out of 16 replicate populations and 4 out of 16  
 119 replicate populations survive, respectively (Fig 3). The likely explanation as to why some populations  
 120 survive and others collapse is due to the stochastic nature of phage adsorption after inoculation: If  
 121 the population composition is close to the herd immunity threshold a stochastic excess of phage  
 122 particles adsorbing to susceptible cells may trigger an epidemic, whereas if chance increases the  
 123 number of phages adsorbing to resistant individuals, the epidemic is suppressed. However, when  
 124 populations have fewer than 96.9% resistant individuals all 16 replicate populations fail to survive  
 125 and collapse under the epidemic (Fig 3).

126 As mentioned in the introduction, phage and bacterial physiology may affect the herd immunity  
 127 threshold. To test this we altered bacterial growth by reducing the concentration of nutrients in the  
 128 medium (Fig 6) which concurrently alters the T7 phage's latent period and burst size (Fig 4A,B and  
 129 Table 2). Indeed, we observe as bacterial growth rates decline the fraction of resistant individuals  
 130 necessary for population survival decreases (Fig 4C). When the populations are grown in a 50%  
 131 diluted growth medium, the fraction of resistant individuals required for a 100% probability of  
 132 survival is 99.2%; when the fraction of resistant individuals is 75% or less populations go extinct. In  
 133 a 20% growth medium the fraction of resistant individuals required for survival decreases to 96.9%,  
 134 while the fraction when all replicates collapse to 50%.

135 From the experimental observations of the herd immunity threshold values we infer the phage  
 136  $R_0$  using Eqn. 1. In an undiluted growth medium the phage  $R_0$  falls between 32 and 256 and  
 137 decreases to between 4 and 128 in 50% and between 2 and 32 in 20% nutrient medium. These data  
 138 indicate that bacterial populations can exhibit herd immunity in homogeneous liquid environments.  
 139 However, bacteria typically live in spatially structured environments such as surfaces, biofilms or  
 140 micro-colonies, therefore we extended our experiments to consider the potential impact of spatially  
 141 structured populations.

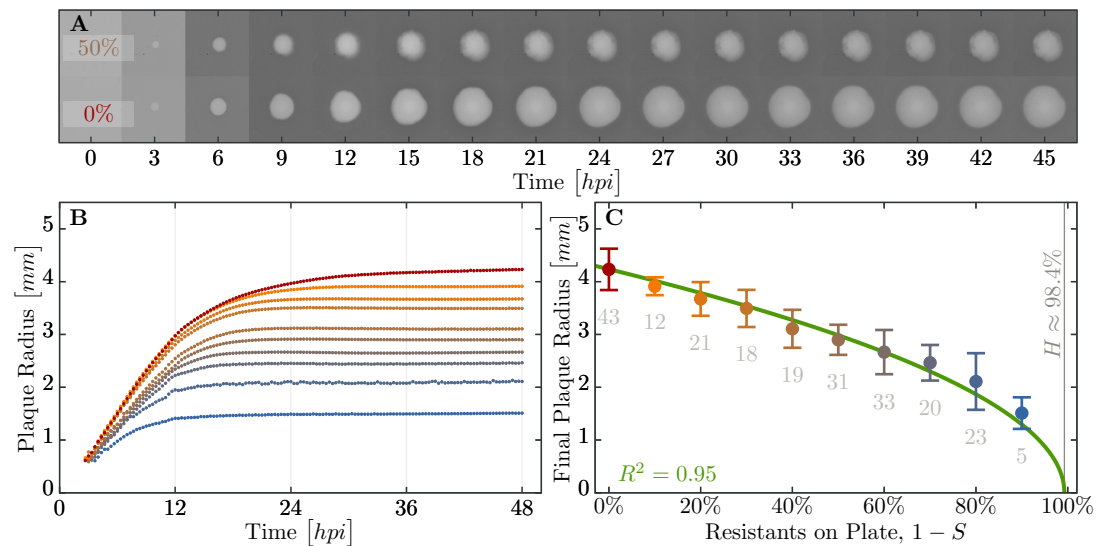


**Figure 5. Properties of expanding phage epidemics on bacterial lawns.** (A) Example of plaque morphology and size change over 48 hours for populations with 50% resistant cells (top) and a control with 100% susceptible cells (bottom). (B) Mean plaque size area through time. Colors indicate the different fraction of resistant individuals (color coding as in panel C). Note the distinct two phases of plaque growth - initially, phage grow fast with exponentially growing bacteria but slow once the nutrients are depleted ( $\approx 10$  hours). The plaque radius is reduced, relative to 100% susceptible population, even when only a small fraction of resistant individuals are in the population. (C) Final plaque radius at 48 hpi. Green line shows the prediction from the model for the plaque radius  $r$ . Grey numbers indicate the number of plaques measured. Error bars indicate the standard deviations.

### 142 Herd immunity in spatially structured populations

143 In order to discern the role, if any, spatial structure plays in herd immunity we conducted a set of  
 144 experiments in spatially structured bacterial lawns on agar plates. Spatially structured bacterial  
 145 populations provide a more fine grained measure of herd immunity, compared to the population  
 146 survival assays done in liquid culture. On bacterial lawns, phages spread radially from a single  
 147 infectious phage particle and the radius of plaque growth on different proportions of resistant to  
 148 susceptible individuals can be easily quantified. In addition, these data allow for estimating the  
 149 speed of the epidemic wave front in these different regimes using real-time imaging (Fig 5A).

150 We observe a decline in the number of plaque forming units (data not shown) and a significant  
 151 decrease in final plaque sizes as the proportion of resistant individuals in the populations increases  
 152 (Fig 5B,C). A reduction in the final plaque size compared to a fully susceptible population was  
 153 statistically significant with as few as 10% resistant individuals in a population ( $p = 0.004$ ,  $t_{53,0.05} =$   
 154  $2.744$ ). In order to determine the effect of resistant individuals during the earlier phase of bacterial  
 155 growth (until the bacterial density on the agar plate reaches saturation; Fig 6A), we analyze the  
 156 velocities of plaque growth between 0 and 24 hours post inoculation (hpi). We find that the speed  
 157 is significantly reduced after 11 hpi when the population consists of as few as 10% of resistant  
 158 individuals ( $p = 0.0317$ ,  $t_{32,0.05} = 1.923$ ). As the fraction of resistant individuals further increases, the  
 159 speed declines significantly at earlier and earlier time points: 6 hpi with 20% ( $p = 0.0392$ ,  $t_{62,0.05} = 1.79$ ),  
 160 and 5.67 hpi with 30% ( $p = 0.0286$ ,  $t_{53,0.05} = 1.943$ ). In fact, when the fraction of resistant individuals  
 161 exceeds 40%, the reduction in the speed of the spread is statistically significant immediately after  
 162 the plaques are visually detectable (Fig 7). It should be noted that all populations with such low  
 163 percentages of resistant individuals in liquid environment collapsed, indicating that spatial structure  
 164 significantly facilitates herd immunity.

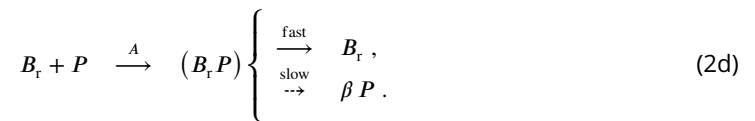
165 The results presented in this and the previous section would allow us to use Eq. (1) to infer a  
 166 value for  $R_0$  from the observed threshold between surviving and collapsing bacterial populations,  
 167 Figs 3 and 4. We also observe that herd immunity is strongly influenced by spatial organization of

168 the population, Fig 5. How the exact value of  $H$  (and subsequently the “classical” epidemiological  
 169 parameter  $R_0$ ) is affected by various factors such as bacterial growth rate, phage burst size and  
 170 latent period is, however, difficult to resolve experimentally. Similarly, quantification of the effect of  
 171 spatial structure is hardly achievable solely by experimental investigation. In order to disentangle  
 172 the roles of all the factors mentioned above, we proceed with development and analysis of a  
 173 mathematical model of the experimental system.

### 174 Modelling bacterial herd immunity

175 We developed a model of phage growth that takes several physiological processes into account:  
 176 bacterial growth during the experiment, bacterial mortality due to phage infection, and phage  
 177 mortality due to bacterial immunity. Furthermore, we use the previously reported observation that  
 178 phage burst size  $\beta$  and latent period  $\lambda$  depend strongly on the bacterial growth rate  $\alpha$  (see Table 1).

179 The main processes in our model system can be defined by the following set of reactions,



180 Susceptible ( $B_s$ ) and resistant ( $B_r$ ) cells grow at a rate  $\alpha$  (no significant difference in growth rate  
 181 between strains,  $p = 0.066$ ,  $t_{70,0.05} = 1.867$ ), (2a) and (2b), by using an amount  $Y$  of the nutrients  $N$ .  
 182 Phage infection first involves adsorption to host cells, (2c) and (2d), with the adsorption term  $A$   
 183 specified below. Infected susceptible bacteria produce on average  $\beta$  phage with a rate inversely  
 184 proportional to the average latency  $\lambda$ . In contrast, resistant bacteria either survive by restricting  
 185 phage DNA via their CRISPR-Cas immune system or – less likely – succumb to the phage infection.  
 186 However, when the MOI is large even resistant cells become susceptible to lysis resulting in the  
 187 release of phage progeny (see Fig 2) [Westra et al. \(2015\)](#); [Chabas et al. \(2016\)](#).

188 In our system, bacteria eventually deplete the available nutrients,  $N(t > T_{\text{depl}}) = 0$ , resulting in  
 189 the cessation of growth. This decline in bacterial growth affects phage growth – latency increases  
 190 and burst size decreases, such that phage reproduction declines dramatically (see Table 2). We  
 191 define the critical time point at which cells transition from exponential growth to stationary phase  
 192 as,

$$T_{\text{depl}} \approx \frac{1}{\alpha} \log \left( \frac{B_{\infty}}{B_0} \right). \quad (3)$$

193 Here,  $B_0$  and  $B_{\infty}$  are the initial and final bacterial densities, respectively. In the initial exponential  
 194 growth phase, our estimates from experimental data for growth parameters are  $\alpha = 0.63 \text{ h}^{-1}$ ,  $\beta =$   
 195  $85.6 \text{ phages/cell}$  and  $\lambda = 0.60 \text{ h}$ , for bacteria and phages, respectively (Table 1 and Table 2). After time  
 196  $T_{\text{depl}}$ , bacterial growth rate is set to zero ( $\alpha = 0$ ) and phage growth is reduced to  $\beta_{\text{depl}} = 3.0 \text{ phages/cell}$   
 197 and  $\lambda_{\text{depl}} = 1.69 \text{ h}$ . Such a two state model – constant growth rate while nutrients are present and no  
 198 growth after depletion – describes the observed population trajectories in experiments quite well  
 199 (see Fig 6).

### 200 Modelling herd immunity in populations without structure

201 An important parameter for estimating herd immunity is the fraction  $S$  of susceptible bacteria in  
 202 the population. As a first estimate, a phage infection spreads in well mixed bacterial cultures if  
 203  $\beta S > 1$  for a continuous chain of infections: the product of burst size  $\beta$  of phage particles and the  
 204 probability  $S$  of infecting a susceptible host has to be larger than one. As a first approximation,  
 205 one could identify  $R_0$  with the burst size  $\beta$ , which is compatible with the observed herd immunity  
 206 thresholds when inverting Eq. (1).

207 However, the growing bacterial population could outgrow the phage population, if the former  
208 reproduces faster, which introduces deviations from the simple relation between  $R_0$  and  $H$  as  
209 shown in (1). We capture this dynamical effect in a correction to the previous estimate as  $\beta S > 1 + \lambda\alpha$   
210 (see Materials and Methods): more phages have to be produced for the chain of infections to persist  
211 in growing populations. The correction  $\frac{\lambda}{1/\alpha}$  is the ratio of generation times of phages over bacteria –  
212 usually, such a correction is very small for non-microbial hosts and can be neglected. Ultimately,  
213 herd immunity is achieved if the threshold defined by  $H = 1 - S_c$  is exceeded, with  $S_c$  the critical  
214 value in the inequality above. Rearranging, we obtain an expression for the herd immunity threshold  
215

$$H = \frac{\beta - 1 - \lambda\alpha}{\beta} . \quad (4)$$

216 This estimate of  $H$  coincides to a very good extent with the population compositions of susceptible  
217 and resistant bacteria where we observe the transition from surviving and collapsed populations in  
218 experiments (see Fig 3). Simulations presented in the Appendix (section Simulation of recovery rate)  
219 show a range in the bacterial population composition with non-monotonic trajectories for  $B_s$  and  
220  $B_r$  (see Fig 9B), which is comparable to the range in composition we find both outcomes, i.e., some  
221 surviving and some collapsing populations in experiments. For such parameter choices, stochastic  
222 effects could then decide the observed fates of bacteria.

223 As presented above, the herd immunity threshold changes when the bacterial cultures grow in a  
224 diluted growth medium. In a set of independent experiments we measured bacterial growth rate  $\alpha$ ,  
225 phage burst size  $\beta$  and phage latent period  $\lambda$  under such conditions (see Fig 6B and Table 2). From  
226 these data we estimated the dependence of the phage burst size on the bacterial growth rate,  $\beta(\alpha)$ ,  
227 using a numerical quadratic fit (Fig 4A). Similarly, we estimated the dependence of the phage latent  
228 period on the bacterial growth rate,  $\lambda(\alpha)$  (Fig 4B). Using these estimates we calculated the expected  
229 growth rate-dependent herd immunity threshold

$$H(\alpha) = \frac{\beta(\alpha) - 1 - \lambda(\alpha)\alpha}{\beta(\alpha)} , \quad (5)$$

230 which gives a very good prediction of the shift in the herd immunity threshold to lower values  
231 for slower growing populations (green line in Fig 4C). This verification of our model shows that it  
232 correctly captures the dependence of the herd immunity threshold on bacterial and phage growth  
233 parameters.

### 234 **Modelling herd immunity in spatially structured populations**

235 The dynamics of phage spread differ between growth in unstructured (e.g., liquid) and structured  
236 (e.g., plates) populations. In order to quantify the effect of spatial structure in a population, we  
237 extend our model to include a spatial dimension. In structured populations growth is a radial  
238 expansion of phages defined by the plaque radius  $r$  and the expansion speed  $v$ , for which several  
239 authors have previously derived predictions *Kaplan et al. (1981)*; *Yin and McCaskill (1992)*; *You and*  
240 *Yin (1999)*; *Fort and Méndez (2002a)*; *Ortega-Cejas et al. (2004)*; *Abedon and Culler (2007)*; *Mitarai*  
241 *et al. (2016)*.

242 We assume phage movement can be captured by a diffusion process characterized with a  
243 diffusion constant  $D$ , which we estimate in independent experiments as  $D = 1.17 (\pm 0.26) \cdot 10^{-2} \text{ mm}^2/\text{h}$   
244 (see Materials and Methods, Fig 8). However, we assume that only phages disperse and bacteria are  
245 immobile as the rate of bacterial diffusion does not influence the expanding plaque on timescales  
246 relevant in the experiment. Adsorption of phages on bacteria is modeled with a adsorption constant  
247  $\delta^*$ . The spreading infection will sweep across the bacterial lawn with the following speed

$$v = 2\sqrt{D\delta^*} \sqrt{\beta S - 1 - \lambda\alpha} , \quad (6)$$

248 which is computed in more details in the Materials and Methods. This expression (6) indicates that  
249 the population composition crucially influences the spreading speed at much lower fractions of



250 resistant bacteria than the herd immunity threshold (4), where phage expansion stops completely.  
251 Consequently, the resulting plaque radius  $r$  decays with increasing fractions of resistants and  
252 reaches zero at  $H$ . A prediction for  $r$  can be obtained by integrating (6) over time. Using the  
253 resulting expression we estimated the adsorption constant  $\delta^*$  from the growth experiments as it is  
254 difficult in practice to measure on plates. The green line in Fig 5B is the best fit, yielding the value  
255  $\delta^* = 4.89(\pm 0.19) \cdot 10^{-2}$  bacteria/phage  $h$  for the adsorption constant.

256 Our results for spatially structured populations allows us to speculate on a general epidemiological  
257 question: If an infection is not stopped by herd immunity in a partially resistant population, by  
258 how much is its spread slowed down? By generalizing (6) we can derive a relative expansion speed,  
259 compared to a fully susceptible population,

$$v_{\text{rel}} = \sqrt{1 - \frac{1 - S}{H}}. \quad (7)$$

260 This expression, (7), is devoid of any (explicit) environmental conditions, which are not already  
261 contained in the herd immunity threshold  $H$  itself. Thus, it could apply to any pathogen-host  
262 system. Ultimately, this relative speed approaches zero with a universal exponent of  $1/2$ , when  
263 the fraction of resistant individuals  $1 - S$  approaches the herd immunity threshold  $H$ . However, a  
264 few caveats exist when using (7), as several conditions have to be fulfilled: Obviously, a pathogen  
265 is expected not to spread in a population exhibiting complete herd immunity – the relative speed  
266 should only hold for populations below the herd immunity threshold. Moreover, if dispersal cannot  
267 be described by diffusion, but rather dominated by large jumps *Hallatschek and Fisher (2014)*,  
268 the diffusion approach we used for traveling waves is not applicable, and thus also renders (7)  
269 inadequate.

## 270 Discussion

271 The spread of a pathogen may be halted or slowed by resistant individuals in a population and  
272 thus provide protection to susceptible individuals. This process, known as herd immunity, has  
273 been extensively studied in a wide diversity of higher organisms *Jeltsch et al. (1997)*; *Mariner et al.*  
274 *(2012)*; *Boven et al. (2008)*; *Meister et al. (2008)*; *Konrad et al. (2012)*; *Wang et al. (2013)*. However,  
275 the role of this process has largely been ignored in microbial communities. To delve into this we  
276 set out to determine under what conditions, if any, herd immunity might arise during a phage  
277 epidemic in bacterial populations as it could have profound implications for the ecology of bacterial  
278 communities.

279 We show that herd immunity can occur in phage-bacterial communities and that it strongly de-  
280 pends on bacterial growth rates and spatial population structure. Average growth rates of bacteria  
281 in the wild have been estimated as substantially slower than in the laboratory (generation time is  
282  $\approx 6.5$  fold longer *Gibson et al. (2016)*), a condition that we have shown to facilitate herd immunity.  
283 Furthermore, bacterial populations in the wild are also highly structured, as bacteria readily form  
284 micro-colonies or biofilms *Hall-Stoodley et al. (2004)* and grow in spatially heterogeneous environ-  
285 ments such as soil or the vertebrate gut *Fierer and Jackson (2006)*, a second condition we have  
286 shown to facilitate herd immunity. These suggest that herd immunity may be fairly prevalent in low  
287 nutrient communities such as soil and oligotrophic marine environments.

288 In an evolutionary context, herd immunity may also impact the efficacy of selection as the  
289 selective advantage of a resistance allele will diminish as the frequency of the resistant allele in  
290 a population approaches the herd immunity threshold,  $H$ . This has two important implications.  
291 First, while complete selective sweeps result in the reduction of genetic diversity at linked loci, herd  
292 immunity may lead to only partial selective sweeps in which some diversity is maintained. Second,  
293 herd immunity has a potential to generate and maintain polymorphism at immunity loci, as has been  
294 shown for genes coding for the major histocompatibility complex (MHC) *Wills and Green (1995)*.  
295 Polymorphism in CRISPR spacer contents have been demonstrated in various bacterial *Tyson and*  
296 *Banfield (2008)*; *Sun et al. (2016)*; *Kuno et al. (2014)* and Archaeal *Held et al. (2010)* populations and

297 communities *Pride et al. (2011); Zhang et al. (2013); Andersson and Banfield (2008)*. While these  
298 studies primarily explain polymorphisms in CRISPR spacer content as a result of rapid simultaneous  
299 independent acquisition of new spacers, we suggest that observed polymorphisms may result from  
300 frequency-dependent selection on resistance loci arising from herd immunity. It has also been  
301 suggested that herd immunity might favor stable coexistence between hosts and their pathogens  
302 *Hamer (1906); Fine (1993); Childs et al. (2014)*.

303 We also developed a mathematical model and show how the herd immunity threshold  $H$   
304 (Eqn. (4)) depends on the phage burst size  $\beta$  and latent period  $\lambda$ , and on the bacterial growth rate  $\alpha$ .  
305 This dependence arises as phages have to outgrow the growing bacterial population, as host and  
306 pathogen have similar generation times in our microbial setting. In addition to these parameters,  
307 we also describe how the speed  $v$  (Eqn. (6)) of a phage epidemic in spatially structured populations  
308 depends on phage diffusion constant  $D$ , phage adsorption rate  $\delta^*$ , and the fraction of resistant and  
309 susceptible individuals in the population. All of which are likely to vary in natural populations. We  
310 also derived the relative speed of spread for partially resistant populations, as measured relative to  
311 a fully susceptible population, and show that it can be parametrized solely with the herd immunity  
312 threshold  $H$  (Eqn. (7)). This relative speed of the spread of an epidemic should be applicable to any  
313 spatially structured host population where the spread of the pathogen can be approximated by  
314 diffusion. Both our experiments and the modelling show that even when the fraction of resistant  
315 individuals in the population is below the herd immunity threshold the expansion of an epidemic  
316 can be substantially slowed, relative to a fully susceptible population.

317 In conclusion, we have presented an experimental model system and the connected theory that  
318 can be usefully applied to both microbial and non-microbial systems. Our theoretical framework  
319 can be useful for identifying critical parameters, such as  $H$  (and to some extent  $R_0$ ), from the  
320 relative speed of an epidemic expansion in partially resistant populations so long as the process  
321 of pathogen spread can be approximated by diffusion. This approximation has been shown to  
322 be useful in such notable cases as rabies in English foxes *Murray et al. (1986)*, potato late blight  
323 *Scherm (1996)*, foot and mouth disease in feral pigs *Pech and McIlroy (1990)*, and malaria in humans  
324 *Gaudart et al. (2010)*.

## 325 **Materials and Methods**

### 326 **Experimental methods**

#### 327 Engineering resistance

328 Oligonucleotides AACTTCGGGAAGCACTTGTGGAAG and AAAACTCCACAAGTGCTTCCCGAA were  
329 ordered from Sigma-Aldrich, annealed and ligated into pCas9 plasmid (pCas9 was a gift from  
330 Luciano Marraffini, Addgene plasmid #42876) carrying a *Streptococcus pyogenes* truncated CRISPR  
331 type II system. For the detailed protocol see *Jiang et al. (2013)*. The oligonucleotides were chosen  
332 so that the CRISPR system targets an overlap of phage T7 genes 4A and 4B. Therefore, the CRISPR  
333 system allows the gene 0.7, coding for a protein which inhibits the RNA polymerase of the cell, to be  
334 expressed before the T7 DNA gets cleaved *García and Molineux (1995)*. The subsequent growth of  
335 the cells is halted and phage replication is inhibited. The plasmid was electroporated into *Escherichia*  
336 *coli* K12 MG1655 (F- lambda- *ilvG-rfb-50 rph-1*). The T7 wildtype phage was used in all experiments.

#### 337 Efficiency of the CRISPR-Cas system

338 Efficiency of the engineered CRISPR-Cas system was tested using the following protocol: Overnight  
339 culture was diluted 1 in 10, cells were infected with the T7 phage and incubated for 15 min in 30°C.  
340 Cells were spun down for 2 min in room temperature at 21130g. Supernatant was discarded and the  
341 cell pellet was resuspended in 950  $\mu$ l of 1X Tris-HCl buffer containing 0.4% ( $\approx 227 \mu$ M) ascorbic acid  
342 pre-warmed to 43°C and incubated in this temperature for 3 min to deactivate free phage particles  
343 *Murata and Kitagawa (1973)*. Cultures were serially diluted and plated using standard plaque assay  
344 protocol on a bacterial lawn of susceptible cells to detect bursting infected cells. The supernatant  
345 was tested for free phage particles, which were not detected.

346 Determining the mean number of phages per cell

347 The cultures that were plated using standard plaque assays in the “Efficiency of the CRISPR-Cas  
348 system” experiment were also plated on LB agar plates containing 25  $\mu\text{g}/\text{ml}$  chloramphenicol to  
349 determine the number of surviving CFUs. The numbers of bursting and surviving susceptible cells  
350 were subsequently used to determine the actual mean number of adsorbed phages per cell. The  
351 fraction of susceptible cells surviving the phage challenge experiment was assumed to correspond  
352 to the Poisson probability that a cell does not encounter any phage, which was then used to  
353 determine the mean of the Poisson distribution, which corresponds to the mean number of phages  
354 per cell.

355 Herd immunity in a liquid culture

356 Herd immunity in a liquid culture was tested in 200  $\mu\text{l}$  of LB broth supplemented with 25  $\mu\text{g}/\text{ml}$   
357 chloramphenicol in Nunclon flat bottom 96 well plate in a Bio-Tek Synergy H1 Plate reader. Bacterial  
358 cultures were diluted 1 in 1000 and mixed in the following ratios of resistant to susceptible cells:  
359 50:50, 75:25, 87.5:12.5, 93.75:6.25, 96.88:3.13, 98.44:1.56, 99.22:0.78, 99.61:0.39, 99.8:0.2, 99.9:0.1,  
360 99.95:0.05, 100:0 %. T7 phage was added at a multiplicity of infection (MOI) of  $\approx 10^{-4}$  ( $\approx 50$  plaque  
361 forming units (*pfu*) per culture) to resemble an epidemic initiated by the burst size from one infected  
362 cell and the cultures were monitored at an optical density 600 nm for 18 hours post inoculation  
363 (*hpi*).

364 Time-lapse imaging of plaque growth

365 Soft LB agar (0.7%) containing 25  $\mu\text{g}/\text{ml}$  chloramphenicol was melted and poured into glass test  
366 tubes heated to 43°C in a heating block. After the temperature equilibrated, 0.9 ml of a bacterial  
367 culture consisting of resistant and susceptible cells (ratios 10% – 100% of susceptible cells, 10%  
368 increments) were diluted 1 in 10 and added to the tubes. Then, 100  $\mu\text{l}$  of bacteriophage stock,  
369 diluted such that there would be  $\approx 10$  plaques per plate, was added to the solution. Tubes were vor-  
370 texed thoroughly and poured as an overlay on LB agar plates containing 25  $\mu\text{g}/\text{ml}$  chloramphenicol.  
371 The plates were placed on scanners (Epson Perfection V600 Photo Scanner) and scanned every 20  
372 minutes in “Wide Transparency mode” for 48 hours. A total of 3 scanners were employed with a  
373 total of 12 plates, plus a no phage control plate and 100% resistant control outside the scanners  
374 (see Fig 10). Time-lapse images were used to calculate the increase of individual plaque areas using  
375 image analysis software PerkinElmer Volocity v6.3.

376 Bacterial growth on soft agar

377 Growth rate of susceptible bacteria in soft LB agar (0.7%) was measured by sampling from a petri  
378 dish with a soft agar overlay with bacteria prepared in the same way as the plaque assays except  
379 an absence of the phage. Sampling was performed in spatially randomized quadruplicates at the  
380 beginning of the experiment and subsequently after 2, 4, 6, 8, 10, 12, 14, 16, 24, 32, 40, and 48  
381 hours using sterile glass Pasteur pipettes (Fisherbrand art.no.: FB50251). Samples were blown  
382 out from the Pasteur pipette using an Accu-jet pro pipettor into 1 ml of M9 buffer pre-warmed  
383 to 43°C, vortexed for 15 seconds and incubated for 10 minutes in 43°C with two more vortexing  
384 steps after 5 and 10 minutes of incubation. Samples were serially diluted and plated on LB agar  
385 plates containing 25  $\mu\text{g}/\text{ml}$  chloramphenicol. How bacterial densities change over time, measured  
386 as CFU/ml, is shown in Fig 6A.

387 Bacterial growth rates in liquid culture

388 Nutrient-dependent growth rate of susceptible bacteria was measured in Nunclon flat bottom 96  
389 well plate in Bio-Tek Synergy H1 Plate reader in 30°C. Overnight LB cultures were diluted 1:200 in  
390 media consisting of LB broth mixed with 1X M9 salts in ratios 10:90, 20:80, 30:70, 40:60, 50:50, 60:40,  
391 70:30, 80:20, 90:10 and 100:0. Final volume was 200  $\mu\text{l}$ . Optical density at 600 nm was measured  
392 every 10 min. Natural logarithm of the optical density values was calculated to determine the  
393 growth rate using a maximal slope of a linear regression of a sliding window spanning 90 min.

	Estimate	Units
$\alpha_{\max}$	0.720 ( $\pm 0.011$ )	$[h^{-1}]$
$K_c$	0.257 ( $\pm 0.012$ )	Dilution $N$ of LB [0... 1]

**Table 1. Estimated parameters for bacterial growth using Monod kinetics.** Undiluted LB medium ( $N = 1$ ) is assumed to have 15 mg/ml nutrients (10 mg/ml Tryptone, 5 mg/ml yeast extract). The full dataset is shown in Fig 6.

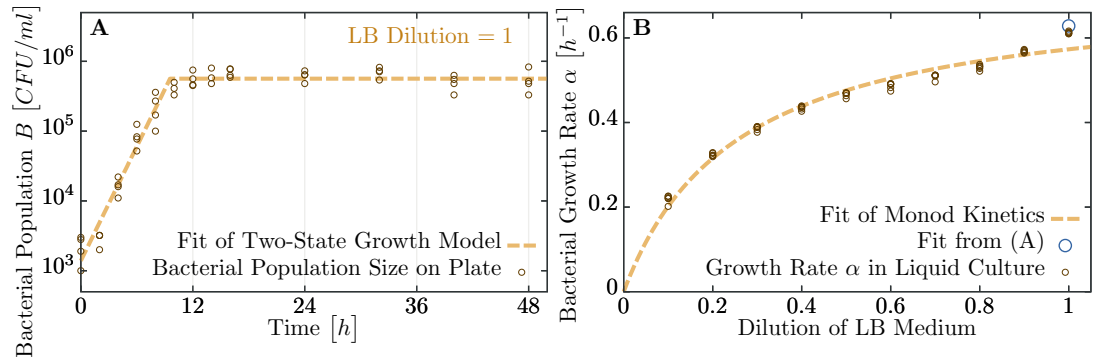


**Figure 6. Measuring bacterial growth without phage.** (A) Trajectory of population size on agar plates over time. For modeling, we assume two states of growth (green curve): first, the bacterial population grows exponential until the time  $T_{\text{depl}}$ , when nutrients are depleted. From this time on, growth rate is assumed to be zero and the population saturates at a maximal size  $B^{\text{final}}$ . Experimental observations fit this proposed growth curve to a very good extent. After all, half of all nutrients are used up in the last generation – with generation times of less than one hour, this the switch between growth and no-growth should be fast. (B) Growth rates of bacteria in diluted medium follow closely Monod's empirical law, given by expression (8). Fit parameters are found to be  $\alpha_{\max} \approx 0.720 h^{-1}$  and  $K_c \approx 0.257$  (with the latter in dimensionless units as dilution of LB medium), see also Table 1.

Medium	Dilution $N$	Latent period $\lambda$ [min]	Burst size $\beta$	Burst size/hour $\beta/\lambda$ [ $h^{-1}$ ]
LB 0	0.0	101.1 ( $\pm 10.9$ )	3.0 ( $\pm 1.9$ )	1.8 ( $\pm 1.1$ )
LB 20	0.2	43.4 ( $\pm 3.9$ )	12.0 ( $\pm 4.2$ )	16.6 ( $\pm 6.0$ )
LB 50	0.5	40.0 ( $\pm 3.0$ )	35.6 ( $\pm 16.4$ )	53.4 ( $\pm 24.9$ )
LB 100	1.0	36.1 ( $\pm 6.1$ )	85.6 ( $\pm 47.3$ )	142.1 ( $\pm 82.1$ )

**Table 2. Estimated parameters for phage growth.** See also Fig 4A,B.

394 The resulting growth rates for various nutrient concentrations fit well with Monod's growth  
 395 kinetics,

$$\alpha = \alpha_{\max} \frac{N}{K_c + N} \quad (8)$$

396 Results for the two fitting parameters,  $\alpha_{\max}$  and  $K_c$ , are listed in Table 1. The whole dataset, including  
 397 the fit, is displayed in Fig 6B.

398 Test for a difference in growth rates of resistant and susceptible bacteria was done in LB broth  
 399 in the same manner as nutrient-dependent growth rate measurements. Two-sample t-test was  
 400 performed on acquired growth rate data.

401 All growth media used in growth rate measurements were supplemented with 25  $\mu\text{g/ml}$  chlo-  
 402 ramphenicol.

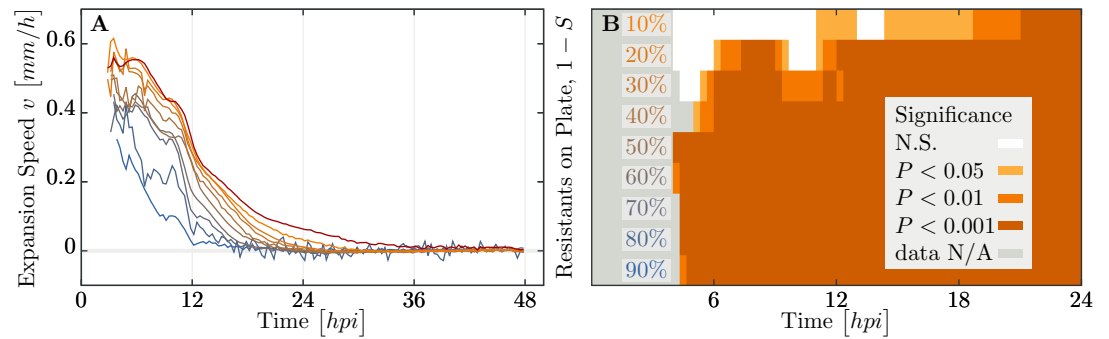


**Figure 7. Speed of phage epidemic expansion on bacterial lawns.** (A) Speed of expanding phage epidemics for all population compositions is initially high, before it drops once nutrients are depleted at around 10 hpi (hours post infection). (B) Plaque speed significance. Comparing velocities of plaque spread with the 100% susceptible control. Linear regression of a sliding window spanning 4 hours of the radius sizes was calculated for all individual plaques and all compositions of the populations between  $t_0$  and  $t_{24}$ . Slopes of the linear regressions for all compositions of the populations were compared using a two-sided heteroscedastic t-test against the 100% susceptible dataset.

#### 403 Phage burst sizes

404 Phage burst sizes in bacteria growing at different growth rates were measured by one-step phage  
405 growth experiments. The burst sizes were calculated as the ratio of average number of plaque  
406 before burst to average number of plaques after burst. Consecutive sampling before and after  
407 burst were used for the calculation if they were not significantly different from each other (two  
408 sided t-test,  $p > 0.05$ ).

#### 409 Phage latent periods

410 Phage latent periods were determined as the time interval between the first and the last significantly  
411 different consecutive sampling between those used for phage burst size calculations.

#### 412 Speed of phage expansion

413 The speed of the phage expansion was measured as difference in radii of plaques over time.  
414 Statistical tests allowed to infer that the reduction of expansion speed is significant already for  
415 small deviations from the 100% susceptible control experiment, as described and shown in Fig. 7.

#### 416 Phage diffusion in soft agar

417 Soft M9 salts soft agar (0.5%) was supplemented with SYBR safe staining (final conc. 1%) and  
418 poured into glass cuvettes (VWR type 6040-OG) to fill  $\sim 2$  cm of the cuvette height. After soft  
419 agar solidification, the same stained soft agar was supplemented with T7 phage particles to a  
420 final concentration  $10^{11}$  pfu/ml and poured on top of the agar without phages. The cuvettes were  
421 monitored in  $30^\circ\text{C}$  every hour for 40 hours at the SYBR safe emission spectrum peak wave length  
422  $524$  nm illuminated with the SYBR safe excitation spectrum peak wave length  $509$  nm. The diffusion  
423 constant was estimated as the best fit parameter for the spread of fluorescent phages through the  
424 soft agar over time.

425 First we computed the luminosity  $L_i$  of fluorescence (a gray-scale value defined as  $L = 0.2126R +$   
426  $0.7152G + 0.0722B$  from the RGB image) as average over the width of the cuvette for pixel row  $i$ , and  
427 corrected the profiles of luminosity  $L_i$  by subtracting the background value. This background value  
428 was estimated as a linear fit at the end of the profile without phages, where only the gray value of  
429 the agar was measured. Moreover, luminosity saturates at values above  $\sim 0.4$  where it does not  
430 have a simple linear dependence on fluorescence: diffusion would lead to a decrease of the signal  
431 behind the inflection point of the profile and increase after the inflection point, but images only  
432 show increasing profiles – the bulk density does not decay. Thus, any estimate should only take the  
433 part of the profile that is below the threshold value of 0.4 into account (see Fig 8).

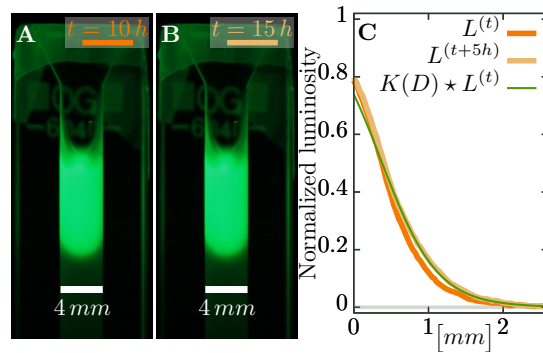


**Figure 8. Estimating diffusion constant of phages.** (A), (B) Phage are slowly expanding on agar which can be observed via their fluorescence. Pictures are taken 5 h apart. (C) The diffusion constant  $D$  can be estimated as best-fit parameter in a *heat kernel*  $K(D)$ :  $K(D)$  propagates the fluorescence profile  $L^{(t)}$  at time  $t$  forward (via a convolution to “smear” out the signal) to the profile  $L^{(t+\Delta t)}$  at the next measured time point. The difference between the expected change and the actual profile is quantified as total squared deviation, see Eqn. (9), which we minimize to obtain  $D$ . Consequently, we can estimate the diffusion constant as  $D \approx 1.17 \cdot 10^{-2} \text{ mm}^2/\text{h}$ . The green line uses this estimated parameter  $D$  and shows the change between the profile at  $t = 10 \text{ h}$  (orange line) and the profile at  $t = 15 \text{ h}$  (light brown line), assuming diffusive spread of phages. See Materials and Methods for more information.

434 The diffusion constant  $D$  itself was estimated as the minimal value of the total squared deviation  
 435 of the convoluted profile  $L^{(t)}$  (at time  $t$ ) with a heat kernel  $K(D)$  compared to the profile  $L^{(t+1)}$  at  
 436 time  $t + 1$ ,

$$D = \left\langle \min_D \sum_i \left( \left( \sum_j \frac{e^{-(i-j)^2/4D}}{\sqrt{4\pi D}} L_j^{(t)} \right) - L_i^{(t+1)} \right)^2 \right\rangle. \quad (9)$$

437 Such a convolution with the heat kernel  $K_{ij}(D) = (4\pi D)^{-1/2} \exp(-(i-j)^2/4D)$  assumes that the only  
 438 change in the profile is due to diffusion for a time span of length 1 with  $i$  and  $j$  indices of pixels.  
 439 Thus, expression (9) estimates the diffusion constant in units of  $\text{pixel}^2/\text{frame}$ , where frame is the  
 440 time difference between two images. Several estimates are averaged over different snapshots in  
 441 the whole experiment that spans 40 h in intervals of 1 h each.

442 The final estimate in appropriate units is

$$D \approx 1.17 (\pm 0.26) \cdot 10^{-2} \text{ mm}^2/\text{h}, \quad (10)$$

443 which is in agreement with previous measures of phage diffusion *Stent and Wollman (1952); Bayer*  
 444 *and DeBlois (1974); Briandet et al. (2008)*.

## 445 Modelling

### 446 Phage growth

447 In the main text we stated that relevant processes for phages growing on bacteria are given by  
 448 the set of reactions (2). In the following, we will analyze an extended version of our model, which  
 449 takes all these processes into account. We try to justify our approximations and explain the  
 450 reasoning behind leaving parts of the full model out. While reactions for single bacteria or phages  
 451 are inherently stochastic in nature, we assume that the involved numbers are large enough such  
 452 that the dynamics can be described with deterministic differential equations for the populations.  
 453 Furthermore, reaction rates are identified with the inverse of the average time scale of the process.

454 Thus, the full model is given by the coupled differential equations,

$$\partial_t B_s = \alpha B_s - A[B_s, P|B_j], \quad (11a)$$

$$\partial_t B_r = \alpha B_r - A[B_r, P|B_j] + \rho I_r, \quad (11b)$$

$$\partial_t I_s = A[B_s, P|B_j] - (1/\lambda)I_s, \quad (11c)$$

$$\partial_t I_r = A[B_r, P|B_j] - (1/\lambda)I_r - \rho I_r, \quad (11d)$$

$$\partial_t P = (\beta/\lambda)(I_s + I_r) - \sum_{i \in \{s,r\}} A[B_i, P|B_j] - \sum_{i \in \{s,r\}} A[I_i, P|B_j], \quad (11e)$$

$$\partial_t N = -\alpha/Y(B_s + B_r). \quad (11f)$$

455 Both bacterial populations  $B_i$  grow with rate  $\alpha$  and decay via adsorption of phages  $A[B_i, P|B_j]$ , an  
 456 expression that is specified below. Infected populations  $I_i$  gain numbers by adsorption and decrease  
 457 via bursting. Resistant bacteria also can recover from their infected state with a recovery rate  $\rho$ .  
 458 Phages grow by bursting cells, and lose numbers by adsorption to the various bacterial populations.  
 459 Moreover, explicit dynamics for nutrients is considered, which are drained by each grown cell  
 460 inversely proportional to the yield  $Y$ , the conversion factor between nutrient concentration and  
 461 cell numbers. Essentially, this last equation acts as a timer, when we switch from abundant  
 462 resources to the depleted state: all growth parameters change significantly upon nutrient depletion.  
 463 Nevertheless, despite the possible deviations, we assume depletion time is given by the simple  
 464 estimate (3) and only treat the two possible states of abundant and depleted nutrients.

465 Adsorption of phages, given by the term  $A[B_i, P|B_j]$ , can be influenced by the whole distribution  
 466 of populations within the culture. In liquid medium, a common assumption is that this term is  
 467 proportional to the concentrations of both the phages and cells **Weitz (2016)**,

$$A[B_i, P|B_j] = \delta B_i P, \quad (12)$$

468 with an adsorption constant  $\delta$ . This expression assumes constant mixing of the population and  
 469 relatively short contact times between phages and bacteria. In general, this system of equations  
 470 is akin to Lotka-Volterra dynamics, which has been analyzed in great detail, eg. **Hofbauer and**  
 471 **Sigmund (1998)**; **Nowak (2006)**.

472 For our ensuing analysis, we neglect the population of infected resistant bacteria  $I_r$ . Upon  
 473 examining (11d) we find that most cells to leave their infected state by reducing phage DNA via  
 474 CRISPR/Cas instead of bursting if  $\rho \gg 1/\lambda$ . If furthermore  $\rho \gg \delta P$ , which is true at least in the  
 475 initial stages of the experiment, essentially all infected resistant bacteria immediately recover from  
 476 a phage infection. Consequently, with both conditions, the resistant infected bacteria tend to  
 477 vanish,  $I_r \rightarrow 0$ , and their dynamics can be neglected. Only in the Appendix (section Simulation of  
 478 recovery rate) we release this assumption to explicitly cover the full dynamics of (11) in simulations  
 479 to estimate values for  $\rho$ .

480 Exponentially growing bacteria lead to double exponential phage growth

481 For convenience, we transform the populations to the total bacterial density  $B = B_s + B_r$  and  
 482 introduce the fraction of susceptible cells  $S = B_s/B$ . The crucial assumption for the remainder  
 483 of this section is that phages burst immediately after infection,  $\lambda = 0$ , such that we can ignore all  
 484 infected populations. While not a very biological condition, it allows to analyze the model in more  
 485 detail. Using these simplifications, we obtain

$$\partial_t B = (\alpha - \delta S P) B, \quad (13a)$$

$$\partial_t S = -S(1 - S)\delta P, \quad (13b)$$

$$\partial_t P = (\beta S - 1)\delta B P. \quad (13c)$$

486 If we assume that in initial stages of phage growth the number of phages is small, ie.  $\delta P \ll \alpha \sim$   
 487  $\mathcal{O}(1 h^{-1})$ , the dynamics of bacteria and the fraction of susceptibles simplify to  $\partial_t B = \alpha B$  and  $\partial_t S = 0$ .

488 Note that this term  $\delta P$  also occurs in the linear phage dynamics, where it cannot be neglected. In  
 489 this instance, we need to view  $\delta B$  as a coefficient, which is likely much larger initially. This set of  
 490 simplified equations can be solved in closed form,

$$S(t) = S_0, \quad (14a)$$

$$B(t) = B_0 \exp(\alpha t), \quad (14b)$$

$$P(t) = P_0 \exp((S_0 \beta - 1) \delta B_0 (\exp(\alpha t) - 1) / \alpha). \quad (14c)$$

491 The structure of phage dynamics is particularly important here – it exhibits a double-exponential  
 492 dependence on time  $t$ , which is a very fast, almost explosive, growth. Such double-exponential  
 493 growth leads to very large population sizes within a short amount of time (but after an extended  
 494 initial delay). This general behavior of the solution is independent of the actual growth rate of  
 495 phages, which only has to be positive. Thus, inspecting the exponent in (14c) yields the condition

$$\beta S_0 > 1 \quad (15)$$

496 for phage growth to be positive. Incidentally, relation (15) is the naive estimate for the number of suc-  
 497 cessful additional infections arising from a single burst. The double exponential time-dependence  
 498 is central for our arguing that the dynamics can be described by threshold phenomena, given by  
 499 conditions like (15): Usually, phages are negligible in the dynamics until they grow fast enough to  
 500 large enough size, such that it is too late for the bacterial population to deal with the overwhelming  
 501 phage population.

502 An important question in the context of these solutions is whether nutrients run out before  
 503 this double-exponential growth of phages occurs. Hence, we compute the time  $T_\delta$  defined as when  
 504 phages reach a population of  $P(T_\delta) = 1/\delta$  assuming phages grow as (14c) until then. After  $T_\delta$  the  
 505 assumptions that allowed to obtain (14c) are not valid anymore. Inverting (14c) for time leads to

$$T_\delta = \frac{1}{\alpha} \log \left( 1 + \frac{\alpha \log(1/\delta P_0)}{(\beta S_0 - 1) \delta B_0} \right). \quad (16)$$

506 Subsequently, we can compare this estimate  $T_\delta$  to the depletion time  $T_{\text{depl}} = (1/\alpha) \log(B_\infty/B_0)$ . When  
 507 rearranging the inequality  $T_{\text{depl}} > T_\delta$  in terms of the (initial) fraction of susceptibles  $S_0$ , we obtain

$$\beta S_0 > 1 + \frac{\alpha \log(1/\delta P_0)}{\delta(B_\infty - B_0)}. \quad (17)$$

508 This expression (17) is a condition for phages to reach “large” population sizes before nutrients  
 509 are depleted by bacteria. The final population density  $B_\infty$  usually fulfills  $\delta B_\infty \gg 1$ , such that the  
 510 correction given by the second term of (17) can be considered small. Thus, if phages grow ( $\beta S_0 > 1$ ),  
 511 they also grow very fast with a double-exponential time-dependence and reach a considerably large  
 512 population size before bacteria stop multiplying (for almost all parameter values).

### 513 Extending analysis to finite burst times

514 The analysis above only treated the case  $\lambda \rightarrow 0$ . However, we reported that the latency time  $\lambda$   
 515 increases significantly when bacterial growth rate  $\alpha$  declines, see Table 2. Considering finite latency  
 516 times entails dealing with an infected bacterial population  $I$ . (However, we identify  $I \equiv I_s$  and set  
 517  $I_r = 0$ .)

518 To this end, note that we can rearrange (11a) to  $(1 + \lambda \partial_t) I = \lambda \delta S B P$  using the adsorption model  
 519 in (12). Hence, we can use the differential operator  $(1 + \lambda \partial_t)$  and apply it directly to (11e) to reduce the  
 520 dependence on  $I$  in this equation at the cost of introducing higher order derivatives. In particular,  
 521 we obtain

$$\lambda \partial_t^2 P + (1 + \lambda \delta B) \partial_t P + \delta B (\beta S - 1 - \lambda \alpha) P = 0, \quad (18)$$

522 where we also inserted  $\partial_t B \approx \alpha B$  in the last term, as we aim again for a solution at initial times  
 523 where  $\delta P \ll \alpha$ . The effects of the limit  $\lambda \rightarrow 0$  are directly observable – no terms are undefined in



524 this limit. In particular, we find that equation (18) and  $\lambda = 0$  lead directly to the dynamics of phages  
525 we just analyzed above, obtaining solution (14c).

526 In principle, (18) is a hyperbolic reaction-diffusion-equation, which is known to occur upon  
527 transformation (or approximation) of time-delayed differential equations **Fort and Méndez (2002b)**.  
528 For initial times we can use the solutions  $B(t) = B_0 \exp(\alpha t)$  and  $S(t) = S_0$ . To proceed, we introduce  
529 the auxiliary variable

$$z(t) = -\delta B_0 \exp(\alpha t) / \alpha, \quad (19)$$

530 and assume  $P(z)$  as a function of this new variable  $z$ . We need to transform the differential operators  
531 of time derivatives, and obtain  $\partial_t = \frac{\partial z(t)}{\partial t} \partial_z = \alpha z \partial_z$  and  $\partial_t^2 = (\alpha z \partial_z)(\alpha z \partial_z) = \alpha^2 (z \partial_z + z^2 \partial_z^2)$ . Inserting  
532 these expressions in (18) and multiplying the whole equation with  $(\alpha^2 \lambda z)^{-1}$  yields the dynamics for  
533 phages,

$$0 = z \partial_z^2 P(z) + (b - z) \partial_z P(z) - a P(z), \quad (20)$$

534 where the two extant constants are  $a = 1 - (\beta S_0 - 1) / (\lambda \alpha)$  and  $b = 1 + 1 / (\lambda \alpha)$ . Equation (20) is called  
535 "Kummers equation" with confluent hypergeometric functions  ${}_1F_1$  as solutions (**Abramowitz and**  
536 **Stegun, 1964**, pg. 504),

$$P(z) = A {}_1F_1(a, b; z) + B z^{1-b} {}_1F_1(a - b + 1, 2 - b; z). \quad (21)$$

537 The two integration constants  $A$  and  $B$  can be determined via the initial conditions  $P(t = 0) = P_0$  and  
538  $(\partial_t P)(t = 0) = -\delta B_0 P_0$ . Using these conditions, the shape of the solution is again similar to before  
539 with  $\lambda = 0$  (double exponential time-dependence), although  $\lambda > 0$  introduces some skew. The most  
540 important aspect of this solution (21) is to compute the parameter combination where it switches  
541 from a decreasing to increasing function over time. A careful analysis reveals that at the parameter  
542 value  $a = 0$  the behavior of the solution changes. Consequently, we find the condition for growing  
543 phage populations,

$$\beta S_0 > 1 + \lambda \alpha, \quad (22)$$

544 which is a non-trivial extension including finite latency times  $\lambda$ .

545 Note, however, that this relation (22) does not indicate a correction to the general epidemiological  
546 parameter  $R_0$ , which can be identified with  $\beta$  in our model. Rather, it shows that a growing  
547 bacterial population requires the phage population to grow even faster for a continuous chain of  
548 infections in an epidemic. The term  $\lambda \alpha$  denotes the ratio of generation times of pathogen over host,  
549 which in most cases is small and negligible compared to 1. For bacteria and phages, however, which  
550 have similar generation times, such a correction is needed to describe the effects of growing host  
551 population sizes. In contrast, many other epidemiological models assume the host population size  
552 constant and only pathogens are increasing (or decreasing) in number.

553 While our result (22) suggest that it also should hold in the limit  $\alpha \rightarrow 0$ , it might not necessarily  
554 be so. This specific limit is actually quite important for the time when nutrients are depleted in the  
555 experiments. However, at several instances in the calculations above we implied a positive  $\alpha > 0$ .  
556 The most important of these is the transformation to  $z(t) = -\delta B(t) / \alpha$ , which actually exhibits two  
557 problems: dividing by  $\alpha$  should not be allowed and  $B(t)$  is essentially constant and cannot serve  
558 as a variable in a differential equation. We also neglected the second term in  $\partial_t B = (\alpha - \delta S P) B$   
559 throughout our calculation. For  $\alpha = 0$  this second term is dominant in bacterial dynamics and would  
560 generate non-linear phage dynamics if inserted for  $\partial_t B$  right before stating (18). However, we expect  
561 that albeit the process will run *very* slow, and might not be measurable in experiments, the simple  
562 condition  $\beta S_0 > 1$  could indicate phage expansion and bacterial decay.

### 563 Growth of phages on plated bacterial lawn

564 Spatial modelling of phage expansion has produced several predictions for how plaque radius  $r$  and  
565 expansion speed  $v$  are influenced by experimentally adjustable parameters **Kaplan et al. (1981)**;  
566 **Yin and McCaskill (1992)**; **You and Yin (1999)**; **Fort and Méndez (2002a)**; **Ortega-Cejas et al. (2004)**;

567 **Abedon and Culler (2007); Mitarai et al. (2016)**. Here, we try to use a minimal model to estimate  
568 these two observables, based on the considerations of previous sections.

569 One of the main complications arises from the fact that all densities in (11) have a spatial  
570 dimension in addition to their time dependence,  $B_i = B_i(\vec{x}, t)$ ,  $i \in \{s, r\}$ . As explained in the main text  
571 we only consider phage diffusion, heterogeneities in all other densities are generated only by phage  
572 growth. The additional spatial dimension imposes a particular contact network between phages  
573 and bacteria, which are not entirely random encounters anymore: One can expect that the size of  
574 the bacterial neighborhood  $\hat{B}$  phages are able to explore is only slightly determined by the actual  
575 density  $B$ , and can be assumed constant for most of the experiment,  $\hat{B}(B) \approx const$ . Consequently,  
576 the adsorption term can be written in the following way,

$$A[B_i, P|B_j] = \delta^* \frac{B_i}{\sum_j B_j} P, \quad (23)$$

577 which only depends on the *relative* frequencies of bacterial strains. The adsorption constant  $\delta^*$  is  
578 both the rate of adsorption and inter-host transit time as determined by the diffusion constant  $D$ .  
579 Thus, one can expect the formal dependence  $\delta^* = \delta^*(D, \hat{B}(B))$ . For our particular experimental  
580 setup, however,  $\delta^*$  will be treated as a constant. This adsorption term (23) leads to the dynamics of  
581 phages

$$\partial_t P = D \nabla^2 P + G[P, S], \quad (24)$$

582 where we collected all contributions to phage growth in  $G[P, S]$  and added the spatial diffusion  
583 term  $D \nabla^2 P$ . For simplicity, we consider only expansion in a single dimension ( $\nabla^2 \equiv \partial_x^2$ ), which has  
584 been found to coincide well with the dynamics of plaque growth **Yin and McCaskill (1992)**. The  
585 growth term for phages is then defined as,

$$G[P, S] = \delta^* (S\beta - 1 - \lambda\alpha) P, \quad (25)$$

586 where we also consider the correction  $\lambda\alpha$  obtained from the analysis in liquid culture. Reaction-  
587 diffusion equations similar to (24) have been first analyzed almost 80 years ago **Fisher (1937)**;  
588 **Kolmogorov et al. (1937)** and since then treated extensively, e.g. **Murray (2002); van Saarloos**  
589 **(2003)**. They admit a traveling wave solution – here, this corresponds to phages sweeping over  
590 an uninfected bacterial lawn. In general, the asymptotic expansion speed for the traveling wave  
591 solutions is given by the following expression,

$$\begin{aligned} v &= 2\sqrt{D(\partial_P G)[0, S]} \\ &= 2\sqrt{D\delta^*} \sqrt{S\beta - 1 - \lambda\alpha}. \end{aligned} \quad (26)$$

592 Only the linearized growth rate of phages at very low densities is relevant for the expansion speed,  
593  $\partial_P G[P = 0, S]$ . Thus, the fraction of susceptible individuals  $S$  should be unchanged from its initial  
594 value  $S_0$ . It should be noted, that only for  $S_0\beta > 1 + \lambda\alpha$  does Eqn. (26) remain valid, otherwise we  
595 have  $v = 0$ . Such a scenario is relevant when nutrients are depleted and phage growth parameters  
596 changes to  $\beta_{\text{depl}}$  and  $\lambda_{\text{depl}}$ .

597 The expression for the expansion speed also shows the need for the spatial adsorption model in  
598 (23), in contrast to the liquid case (12). If adsorption would directly depend on the bacterial density  
599  $B$ , the additional linear dependence on  $B$  in (25) would lead to an exponentially increasing speed  
600 during the experiment. This is in clear contradiction to experimental observations.

601 The density of phages behind the expanding front is large and as previously noted at large  
602 MOIs the CRISPR-Cas system fails to provide effective immunity (see section **Materials and Methods**  
603 and appendix **Infection load and efficiency of the CRISPR/Cas system**). However, in comparison to  
604 an un-structured environment (e.g., liquid) the structured environment effectively limits transit of  
605 phage from within a plaque to the expanding front: The combined effect of growth and diffusion  
606 usually generates a much faster expansion of phages during plaque formation, than diffusion alone.

607 Only when nutrients are depleted, can pure diffusion processes explain the slow decrease in speed  
608 observed in experiments (see Fig 7A). Our model assumes a sharp drop to  $v = 0$  at  $T_{\text{depl}}$  for small  $S$ .

609 In order to derive an expression for the plaque radius  $r$ , we integrate the expansion speed (6)  
610 over time,  $r(t) = \int_0^t dt' v(t')$ . Employing the simplification that only two values of phage growth are  
611 necessary to describe the dynamics – before  $T_{\text{depl}}$  phages grow normally with  $\beta$  and  $\lambda$ , after  $T_{\text{depl}}$   
612 phage growth changes to  $\beta_{\text{depl}}$  and  $\lambda_{\text{depl}}$  – we can evaluate the integral for the radius directly, arriving  
613 at,

$$r(t) = \begin{cases} 2t\sqrt{D\delta^*}\sqrt{S\beta - 1 - \lambda\alpha}, & 0 < t < T_{\text{depl}}, \\ 2\sqrt{D\delta^*}\left(T_{\text{depl}}\sqrt{S\beta - 1 - \lambda\alpha} + (t - T_{\text{depl}})\sqrt{S\beta_{\text{depl}} - 1}\right), & T_{\text{depl}} < t. \end{cases} \quad (27)$$

614 Using this expression we estimated the adsorption constant  $\delta^*$  from the growth experiments as  
615 it difficult to measure in practice. This estimate is done for radii exactly at the time of nutrient  
616 depletion  $T_{\text{depl}}$ , and excluding the control experiment with only susceptible cells.

617 Predictions of our model show a discrepancy from experimental results on plates. We inde-  
618 pendently estimated  $\beta_{\text{depl}} = 3.0$ , which results in  $H_{\text{depl}} = (\beta_{\text{depl}} - 1)/\beta_{\text{depl}} \approx 0.67$ . Thus, all experiments  
619 with  $S > 0.33$  should exhibit expanding plaques after nutrients are depleted. In the experimental  
620 setup plaques stop expanding in all mixtures of resistant to susceptible cells ( $S \leq 0.9$ ), which would  
621 correspond to  $\beta_{\text{depl}} < 1.1$ . This value is, however, still within experimental accuracy of our estimates  
622 of  $\beta_{\text{depl}}$ .

## 623 Acknowledgments

624 We are grateful to Remy Chait for his help and assistance with establishing our experimental setups  
625 and to Tobias Bergmiller for valuable insights into some specific experimental details. We thank  
626 Luciano Marraffini for donating us the pCas9 plasmid used in this study. Finally, we want to express  
627 our gratitude to Seth Barribeau, Andrea Betancourt, Călin Guet, Mato Lagator, Tiago Paixão and  
628 Maroš Pleška for valuable discussions on the manuscript.

## 629 Author Contributions

630 Conceived and designed the experiments: PP JPB. Performed the experiments: PP. Analyzed the  
631 data: PP LG. Conceived and designed the model: PP LG JPB NHB. Encoded and analyzed the model:  
632 LG. Wrote the manuscript: PP LG NHB JPB.

## 633 References

- 634 **Abedon ST**, Culler RR. Optimizing bacteriophage plaque fecundity. *Journal of theoretical biology*. 2007;  
635 249(3):582–592. <http://dx.doi.org/10.1016/j.jtbi.2007.08.006>.
- 636 **Abramowitz M**, Stegun IA. *Handbook of mathematical functions: with formulas, graphs, and mathematical*  
637 *tables*, vol. 55. Courier Corporation; 1964.
- 638 **Anderson RM**, May RM. Directly transmitted infections diseases: control by vaccination. *Science*. 1982 Feb;  
639 215(4536):1053–1060. <http://science.sciencemag.org/content/215/4536/1053>, doi: 10.1126/science.7063839.
- 640 **Anderson RM**, May RM. Spatial, temporal, and genetic heterogeneity in host populations and the design of  
641 immunization programmes. *IMA journal of mathematics applied in medicine and biology*. 1984; 1(3):233–266.
- 642 **Anderson RM**, May RM. Age-related changes in the rate of disease transmission: implications for the design of  
643 vaccination programmes. *The Journal of Hygiene*. 1985 Jun; 94(3):365–436. [http://www.ncbi.nlm.nih.gov/pmc/](http://www.ncbi.nlm.nih.gov/pmc/articles/PMC2129492/)  
644 [articles/PMC2129492/](http://www.ncbi.nlm.nih.gov/pmc/articles/PMC2129492/).
- 645 **Anderson RM**, May RM. *Infectious Diseases of Humans: Dynamics and Control*. OUP Oxford; 1992.
- 646 **Andersson AF**, Banfield JF. Virus Population Dynamics and Acquired Virus Resistance in Natural Microbial  
647 Communities. *Science*. 2008 May; 320(5879):1047–1050. [http://science.sciencemag.org/content/320/5879/](http://science.sciencemag.org/content/320/5879/1047)  
648 [1047](http://science.sciencemag.org/content/320/5879/1047), doi: 10.1126/science.1157358.

- 649 **Bayer M**, DeBlois R. Diffusion Constant and Dimension of Bacteriophage  $\phi$ X174 as Determined by Self-Beat  
650 Laser Light Spectroscopy and Electron Microscopy. *Journal of virology*. 1974; 14(4):975–980.
- 651 **Blumenthal RM**, Cheng X. Restriction-modification systems. *Modern microbial genetics*. 2002; p. 177–225.
- 652 **Boven Mv**, Bouma A, Fabri THF, Katsma E, Hartog L, Koch G. Herd immunity to Newcastle disease virus in  
653 poultry by vaccination. *Avian Pathology*. 2008 Feb; 37(1):1–5. [http://www.tandfonline.com/doi/abs/10.1080/](http://www.tandfonline.com/doi/abs/10.1080/03079450701772391)  
654 [03079450701772391](http://www.tandfonline.com/doi/abs/10.1080/03079450701772391), doi: 10.1080/03079450701772391.
- 655 **Briandet R**, Lacroix-Gueu P, Renault M, Lecart S, Meylheuc T, Bidnenko E, Steenkeste K, Bellon-Fontaine MN,  
656 Fontaine-Aupart MP. Fluorescence correlation spectroscopy to study diffusion and reaction of bacteriophages  
657 inside biofilms. *Applied and environmental microbiology*. 2008; 74(7):2135–2143.
- 658 **Chabas H**, van Houte S, Høyland-Kroghsbo NM, Buckling A, Westra ER; **The Royal Society**. Immigration of  
659 susceptible hosts triggers the evolution of alternative parasite defence strategies. *Proc R Soc B*. 2016;  
660 283(1837):20160721.
- 661 **Childs LM**, England WE, Young MJ, Weitz JS, Whitaker RJ. CRISPR-induced distributed immunity in microbial  
662 populations. *PloS one*. 2014; 9(7):e101710.
- 663 **Destoumieux-Garzón D**, Duquesne S, Peduzzi J, Goulard C, Desmadril M, Letellier L, Rebuffat S, Boulanger P.  
664 The iron-siderophore transporter FhuA is the receptor for the antimicrobial peptide microcin J25: role of  
665 the microcin Val11–Pro16  $\beta$ -hairpin region in the recognition mechanism. *Biochemical Journal*. 2005 Aug;  
666 389(3):869–876. <http://www.biochemj.org/content/389/3/869>, doi: 10.1042/BJ20042107.
- 667 **Fenner F**. Smallpox: emergence, global spread, and eradication. *History and Philosophy of the Life Sciences*.  
668 1993; 15(3):397–420.
- 669 **Ferrari MJ**, Bansal S, Meyers LA, Bjornstad ON. Network frailty and the geometry of herd immunity. *Proceedings*  
670 *of the Royal Society B: Biological Sciences*. 2006 Nov; 273(1602):2743–2748. [http://rspb.royalsocietypublishing.](http://rspb.royalsocietypublishing.org/cgi/doi/10.1098/rspb.2006.3636)  
671 [org/cgi/doi/10.1098/rspb.2006.3636](http://rspb.royalsocietypublishing.org/cgi/doi/10.1098/rspb.2006.3636), doi: 10.1098/rspb.2006.3636.
- 672 **Fierer N**, Jackson RB. The diversity and biogeography of soil bacterial communities. *Proceedings of the National*  
673 *Academy of Sciences of the United States of America*. 2006 Jan; 103(3):626–631. [http://www.pnas.org/content/](http://www.pnas.org/content/103/3/626)  
674 [103/3/626](http://www.pnas.org/content/103/3/626), doi: 10.1073/pnas.0507535103.
- 675 **Fine PE**. Herd immunity: history, theory, practice. *Epidemiologic Reviews*. 1993; 15(2):265–302.
- 676 **Fine P**, Eames K, Heymann DL. “Herd Immunity”: A Rough Guide. *Clinical Infectious Diseases*. 2011 Apr;  
677 52(7):911–916. <http://cid.oxfordjournals.org/content/52/7/911>, doi: 10.1093/cid/cir007.
- 678 **Fisher RA**. The wave of advance of advantageous genes. *Annals of Human Genetics*. 1937; 7(4):355–369.
- 679 **Fort J**, Méndez V. Time-delayed spread of viruses in growing plaques. *Physical review letters*. 2002; 89(17):178101.  
680 <http://dx.doi.org/10.1103/PhysRevLett.89.178101>.
- 681 **Fort J**, Méndez V. Wavefronts in time-delayed reaction-diffusion systems. Theory and comparison to experiment.  
682 *Reports on Progress in Physics*. 2002; 65(6):895.
- 683 **Fox JP**, Elveback L, Scott W, Gatewood L, Ackerman E. Herd immunity: basic concept and relevance to public  
684 health immunization practices. *American Journal of Epidemiology*. 1971 Sep; 94(3):179–189.
- 685 **García LR**, Molineux IJ. Rate of translocation of bacteriophage T7 DNA across the membranes of *Escherichia coli*.  
686 *Journal of Bacteriology*. 1995 Jul; 177(14):4066–4076. <http://www.ncbi.nlm.nih.gov/pmc/articles/PMC177138/>.
- 687 **Gaudart J**, Ghassani M, Mintsá J, Rachdi M, Waku J, Demongeot J. Demography and Diffusion in Epidemics:  
688 Malaria and Black Death Spread. *Acta Biotheoretica*. 2010; 58(2):277–305. [http://dx.doi.org/10.1007/](http://dx.doi.org/10.1007/s10441-010-9103-z)  
689 [s10441-010-9103-z](http://dx.doi.org/10.1007/s10441-010-9103-z), doi: 10.1007/s10441-010-9103-z.
- 690 **Gibson**, Wilson, Feil, Eyre-Walker. personal communication; 2016, unpublished results.
- 691 **Goldfarb T**, Sberro H, Weinstock E, Cohen O, Doron S, Charpak-Amikam Y, Afik S, Ofir G, Sorek R. BREX is a novel  
692 phage resistance system widespread in microbial genomes. *The EMBO journal*. 2015 Jan; 34(2):169–183. doi:  
693 [10.15252/embj.201489455](https://doi.org/10.15252/embj.201489455).
- 694 **Grassly NC**, Fraser C. Mathematical models of infectious disease transmission. *Nature Reviews Microbi-*  
695 *ology*. 2008 Jun; 6(6):477–487. <http://www.nature.com/nrmicro/journal/v6/n6/full/nrmicro1845.html>, doi:  
696 [10.1038/nrmicro1845](https://doi.org/10.1038/nrmicro1845).

- 697 **Hadas H**, Einav M, Fishov I, Zaritsky A. Bacteriophage T4 development depends on the physiology of its host  
698 *Escherichia coli*. *Microbiology (Reading, England)*. 1997 Jan; 143 ( Pt 1):179–185.
- 699 **Hall-Stoodley L**, Costerton JW, Stoodley P. Bacterial biofilms: from the Natural environment to infectious  
700 diseases. *Nature Reviews Microbiology*. 2004 Feb; 2(2):95–108. [http://www.nature.com/nrmicro/journal/v2/](http://www.nature.com/nrmicro/journal/v2/n2/abs/nrmicro821.html)  
701 [n2/abs/nrmicro821.html](http://www.nature.com/nrmicro/journal/v2/n2/abs/nrmicro821.html), doi: 10.1038/nrmicro821.
- 702 **Hallatschek O**, Fisher DS. Acceleration of evolutionary spread by long-range dispersal. *Proceedings of the*  
703 *National Academy of Sciences*. 2014; 111(46):E4911–E4919.
- 704 **Hamer WH**. *Epidemic Disease in England: The Evidence of Variability and of Persistency of Type*. Bedford Press;  
705 1906.
- 706 **Hammad Amm**. Evaluation of alginate-encapsulated *Azotobacter chroococcum* as a phage-resistant and  
707 an effective inoculum. *Journal of Basic Microbiology*. 1998 Mar; 38(1):9–16. [http://onlinelibrary.wiley.](http://onlinelibrary.wiley.com/doi/10.1002/(SICI)1521-4028(199803)38:1<9::AID-JOBM9>3.0.CO;2-4/abstract)  
708 [com/doi/10.1002/\(SICI\)1521-4028\(199803\)38:1<9::AID-JOBM9>3.0.CO;2-4/abstract](http://onlinelibrary.wiley.com/doi/10.1002/(SICI)1521-4028(199803)38:1<9::AID-JOBM9>3.0.CO;2-4/abstract), doi: 10.1002/(SICI)1521-  
709 [4028\(199803\)38:1<9::AID-JOBM9>3.0.CO;2-4](http://onlinelibrary.wiley.com/doi/10.1002/(SICI)1521-4028(199803)38:1<9::AID-JOBM9>3.0.CO;2-4/abstract).
- 710 **Heesterbeek JaP**. A Brief History of  $R_0$  and a Recipe for its Calculation. *Acta Biotheoretica*. 2002 Sep; 50(3):189–  
711 204. <http://link.springer.com/article/10.1023/A%3A1016599411804>, doi: 10.1023/A:1016599411804.
- 712 **Held NL**, Herrera A, Cadillo-Quiroz H, Whitaker RJ. CRISPR Associated Diversity within a Population of *Sul-*  
713 *folobus islandicus*. *PLoS ONE*. 2010 Sep; 5(9). <http://www.ncbi.nlm.nih.gov/pmc/articles/PMC2946923/>, doi:  
714 [10.1371/journal.pone.0012988](http://www.ncbi.nlm.nih.gov/pmc/articles/PMC2946923/).
- 715 **Hofbauer J**, Sigmund K. *Evolutionary games and population dynamics*. Cambridge University Press; 1998.
- 716 **Jeltsch F**, Müller MS, Grimm V, Wissel C, Brandl R. Pattern formation triggered by rare events: lessons from the  
717 spread of rabies. *Proceedings of the Royal Society of London B: Biological Sciences*. 1997 Apr; 264(1381):495–  
718 503. <http://rspb.royalsocietypublishing.org/content/264/1381/495>, doi: 10.1098/rspb.1997.0071.
- 719 **Jiang W**, Bikard D, Cox D, Zhang F, Marraffini LA. RNA-guided editing of bacterial genomes using CRISPR-Cas  
720 systems. *Nature Biotechnology*. 2013; <http://www.nature.com/nbt/journal/vaop/ncurrent/full/nbt.2508.html>,  
721 doi: 10.1038/nbt.2508.
- 722 **Kaplan DA**, Naumovski L, Rothschild B, Collier RJ. Appendix: a model of plaque formation. *Gene*. 1981;  
723 13(3):221–225. [http://dx.doi.org/10.1016/0378-1119\(81\)90027-5](http://dx.doi.org/10.1016/0378-1119(81)90027-5).
- 724 **Kolmogorov AN**, Petrovsky I, Piscounoff N. Study of the diffusion equation with growth of the quantity of  
725 matter and its application to a biology problem. *Bull Univ Moscow, Ser Int A*. 1937; 1(1).
- 726 **Konrad M**, Vyleta ML, Theis FJ, Stock M, Tragust S, Klatt M, Drescher V, Marr C, Ugelvig LV, Cremer S. So-  
727 cial Transfer of Pathogenic Fungus Promotes Active Immunisation in Ant Colonies. *PLOS Biol*. 2012  
728 Apr; 10(4):e1001300. <http://journals.plos.org/plosbiology/article?id=10.1371/journal.pbio.1001300>, doi:  
729 [10.1371/journal.pbio.1001300](http://journals.plos.org/plosbiology/article?id=10.1371/journal.pbio.1001300).
- 730 **Kuno S**, Sako Y, Yoshida T. Diversification of CRISPR within coexisting genotypes in a natural population of  
731 the bloom-forming cyanobacterium *Microcystis aeruginosa*. *Microbiology*. 2014; 160(5):903–916. [http://](http://mic.microbiologyresearch.org/content/journal/micro/10.1099/mic.0.073494-0)  
732 [mic.microbiologyresearch.org/content/journal/micro/10.1099/mic.0.073494-0](http://mic.microbiologyresearch.org/content/journal/micro/10.1099/mic.0.073494-0), doi: 10.1099/mic.0.073494-0.
- 733 **Lloyd AL**, May RM. Spatial Heterogeneity in Epidemic Models. *Journal of Theoretical Biology*. 1996 Mar; 179(1):1–  
734 11. <http://www.sciencedirect.com/science/article/pii/S0022519396900429>, doi: 10.1006/jtbi.1996.0042.
- 735 **Mariner JC**, House JA, Mebus CA, Sollod AE, Chibeu D, Jones BA, Roeder PL, Admassu B, Klooster GGMV'.  
736 Rinderpest Eradication: Appropriate Technology and Social Innovations. *Science*. 2012 Sep; 337(6100):1309–  
737 1312. <http://science.sciencemag.org/content/337/6100/1309>, doi: 10.1126/science.1223805.
- 738 **Meister T**, Lussy H, Bakonyi T, Šikutová S, Rudolf I, Vogl W, Winkler H, Frey H, Hubálek Z, Nowotny N,  
739 Weissenböck H. Serological evidence of continuing high Usutu virus (Flaviviridae) activity and establish-  
740 ment of herd immunity in wild birds in Austria. *Veterinary Microbiology*. 2008 Mar; 127(3–4):237–248.  
741 <http://www.sciencedirect.com/science/article/pii/S0378113507004154>, doi: 10.1016/j.vetmic.2007.08.023.
- 742 **Mitarai N**, Brown S, Sneppen K. Population dynamics of phage and bacteria in spatially structured habitats  
743 using Phage  $\lambda$  and *Escherichia coli*. *Journal of bacteriology*. 2016; 198(12):1783–1793. [http://dx.doi.org/10.](http://dx.doi.org/10.1128/JB.00965-15)  
744 [1128/JB.00965-15](http://dx.doi.org/10.1128/JB.00965-15).

- 745 **Murata A**, Kitagawa K. Mechanism of Inactivation of Bacteriophage J1 by Ascorbic Acid. *Agricultural and*  
746 *Biological Chemistry*. 1973; 37(5):1145–1151. doi: [10.1271/bbb1961.37.1145](https://doi.org/10.1271/bbb1961.37.1145).
- 747 **Murray JD**, Stanley EA, Brown DL. On the Spatial Spread of Rabies among Foxes. *Proceedings of the Royal*  
748 *Society of London B: Biological Sciences*. 1986; 229(1255):111–150. [http://rspb.royalsocietypublishing.org/](http://rspb.royalsocietypublishing.org/content/229/1255/111)  
749 [content/229/1255/111](http://rspb.royalsocietypublishing.org/content/229/1255/111), doi: [10.1098/rspb.1986.0078](https://doi.org/10.1098/rspb.1986.0078).
- 750 **Murray JD**, *Mathematical biology I: an introduction*, Vol. 17 of interdisciplinary applied mathematics. Springer,  
751 New York, NY, USA,; 2002.
- 752 **Nokes DJ**, Anderson RM. Measles, mumps, and rubella vaccine: what coverage to block transmission? *The*  
753 *Lancet*. 1988; 332(8624):1374.
- 754 **Nordström K**, Forsgren A. Effect of Protein A on Adsorption of Bacteriophages to *Staphylococcus aureus*.  
755 *Journal of Virology*. 1974 Aug; 14(2):198–202. <http://jvi.asm.org/content/14/2/198>.
- 756 **Nowak MA**. *Evolutionary dynamics*. Harvard University Press; 2006.
- 757 **Ortega-Cejas V**, Fort J, Méndez V, Campos D. Approximate solution to the speed of spreading viruses. *Physical*  
758 *Review E*. 2004; 69(3):031909. <http://dx.doi.org/10.1103/PhysRevE.69.031909>.
- 759 **Pech RP**, McIlroy JC. A Model of the Velocity of Advance of Foot and Mouth Disease in Feral Pigs. *Journal of*  
760 *Applied Ecology*. 1990; 27(2):635–650. <http://www.jstor.org/stable/2404308>.
- 761 **Pride DT**, Sun CL, Salzman J, Rao N, Loomer P, Armitage GC, Banfield JF, Relman DA. Analysis of strepto-  
762 cocal CRISPRs from human saliva reveals substantial sequence diversity within and between subjects  
763 over time. *Genome Research*. 2011 Jan; 21(1):126–136. <http://genome.cshlp.org/content/21/1/126>, doi:  
764 [10.1101/gr.111732.110](https://doi.org/10.1101/gr.111732.110).
- 765 **Real LA**, Biek R. Spatial dynamics and genetics of infectious diseases on heterogeneous landscapes. *Journal of*  
766 *The Royal Society Interface*. 2007 Oct; 4(16):935–948. <http://rsif.royalsocietypublishing.org/content/4/16/935>,  
767 doi: [10.1098/rsif.2007.1041](https://doi.org/10.1098/rsif.2007.1041).
- 768 **van Saarloos W**. Front propagation into unstable states. *Physics reports*. 2003; 386(2):29–222.
- 769 **Schenzle D**. An Age-Structured Model of Pre- and Post-Vaccination Measles Transmission. *Mathematical*  
770 *Medicine and Biology*. 1984 Jan; 1(2):169–191. <http://imammb.oxfordjournals.org/content/1/2/169>, doi:  
771 [10.1093/imammb/1.2.169](https://doi.org/10.1093/imammb/1.2.169).
- 772 **Scherm H**. On the velocity of epidemic waves in model plant disease epidemics. *Ecological Mod-*  
773 *elling*. 1996; 87(1–3):217 – 222. <http://www.sciencedirect.com/science/article/pii/0304380095000305>, doi:  
774 [http://dx.doi.org/10.1016/0304-3800\(95\)00030-5](http://dx.doi.org/10.1016/0304-3800(95)00030-5).
- 775 **Sorek R**, Lawrence CM, Wiedenheft B. CRISPR-Mediated Adaptive Immune Systems in Bacteria  
776 and Archaea. *Annual Review of Biochemistry*. 2013; 82(1):237–266. [http://dx.doi.org/10.1146/](http://dx.doi.org/10.1146/annurev-biochem-072911-172315)  
777 [annurev-biochem-072911-172315](http://dx.doi.org/10.1146/annurev-biochem-072911-172315), doi: [10.1146/annurev-biochem-072911-172315](https://doi.org/10.1146/annurev-biochem-072911-172315).
- 778 **Stent GS**, Wollman EL. On the two-step nature of bacteriophage adsorption. *Biochimica et biophysica acta*.  
779 1952; 8:260–269.
- 780 **Sun CL**, Thomas BC, Barrangou R, Banfield JF. Metagenomic reconstructions of bacterial CRISPR loci constrain  
781 population histories. *The ISME journal*. 2016; 10(4):858–870. [http://www.nature.com/ismej/journal/v10/n4/](http://www.nature.com/ismej/journal/v10/n4/abs/ismej2015162a.html)  
782 [abs/ismej2015162a.html](http://www.nature.com/ismej/journal/v10/n4/abs/ismej2015162a.html).
- 783 **Sutherland IW**, Hughes KA, Skillman LC, Tait K. The interaction of phage and biofilms. *FEMS microbiology*  
784 *letters*. 2004; 232(1):1–6.
- 785 **Swarts DC**, Jore MM, Westra ER, Zhu Y, Janssen JH, Snijders AP, Wang Y, Patel DJ, Berenguer J, Brouns SJJ, van der  
786 Oost J. DNA-guided DNA interference by a prokaryotic Argonaute. *Nature*. 2014 Mar; 507(7491):258–261.  
787 <http://www.nature.com/nature/journal/v507/n7491/full/nature12971.html>, doi: [10.1038/nature12971](https://doi.org/10.1038/nature12971).
- 788 **Tyson GW**, Banfield JF. Rapidly evolving CRISPRs implicated in acquired resistance of microorganisms to viruses.  
789 *Environmental Microbiology*. 2008 Jan; 10(1):200–207. [http://onlinelibrary.wiley.com/doi/10.1111/j.1462-2920.](http://onlinelibrary.wiley.com/doi/10.1111/j.1462-2920.2007.01444.x)  
790 [2007.01444.x/abstract](http://onlinelibrary.wiley.com/doi/10.1111/j.1462-2920.2007.01444.x), doi: [10.1111/j.1462-2920.2007.01444.x](https://doi.org/10.1111/j.1462-2920.2007.01444.x).
- 791 **Wang Y**, Yang P, Cui F, Kang L. Altered Immunity in Crowded Locust Reduced Fungal ( *Metarhizium anisopliae* )  
792 Pathogenesis. *PLOS Pathog*. 2013 Jan; 9(1):e1003102. [http://journals.plos.org/plospathogens/article?id=10.](http://journals.plos.org/plospathogens/article?id=10.1371/journal.ppat.1003102)  
793 [1371/journal.ppat.1003102](http://journals.plos.org/plospathogens/article?id=10.1371/journal.ppat.1003102), doi: [10.1371/journal.ppat.1003102](https://doi.org/10.1371/journal.ppat.1003102).

- 794 **Weitz JS.** Quantitative Viral Ecology: Dynamics of Viruses and Their Microbial Hosts. Princeton University Press;  
795 2016.
- 796 **Westra ER,** van Houte S, Oyesiku-Blakemore S, Makin B, Broniewski JM, Best A, Bondy-Denomy J, Davidson A,  
797 Boots M, Buckling A. Parasite exposure drives selective evolution of constitutive versus inducible defense.  
798 *Current Biology.* 2015; 25(8):1043–1049.
- 799 **Wills C,** Green DR. A Genetic Herd-Immunity Model for the Maintenance of MHC Polymorphism. *Immunological*  
800 *reviews.* 1995; 143(1):263–292. <http://onlinelibrary.wiley.com/doi/10.1111/j.1600-065X.1995.tb00679.x/full>.
- 801 **Yin J,** McCaskill J. Replication of viruses in a growing plaque: a reaction-diffusion model. *Biophysical journal.*  
802 1992; 61(6):1540. [http://dx.doi.org/10.1016%2FS0006-3495\(92\)81958-6](http://dx.doi.org/10.1016%2FS0006-3495(92)81958-6).
- 803 **Yorke JA,** Nathanson N, Pianigiani G, Martin J. Seasonality and the requirements for perpetuation and eradication  
804 of viruses in populations. *American Journal of Epidemiology.* 1979 Feb; 109(2):103–123.
- 805 **You L,** Yin J. Amplification and spread of viruses in a growing plaque. *Journal of theoretical biology.* 1999;  
806 200(4):365–373. <http://dx.doi.org/10.1006/jtbi.1999.1001>.
- 807 **Zhang Q,** Rho M, Tang H, Doak TG, Ye Y. CRISPR-Cas systems target a diverse collection of invasive mobile genetic  
808 elements in human microbiomes. *Genome Biology.* 2013; 14:R40. <http://dx.doi.org/10.1186/gb-2013-14-4-r40>,  
809 doi: 10.1186/gb-2013-14-4-r40.

## 810 **Appendix: Additional theoretical considerations**

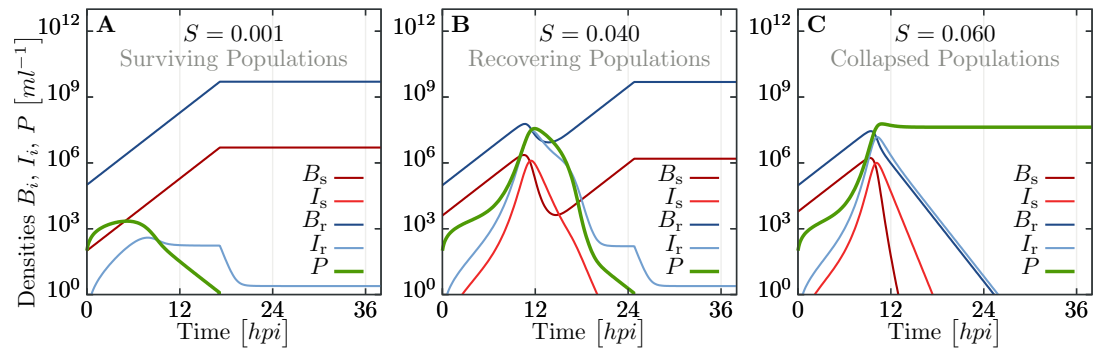
### 811 **Simulation of recovery rate**

812 Throughout the main text we assumed that resistant bacteria are completely immune to phage  
813 infection as their CRISPR/Cas system immediately kills adsorbed phages. However, experimental  
814 observation suggest that for fractions close to what we predicted as herd immunity threshold, *all*  
815 bacteria eventually die. Thus, in the following section we use numerical simulations to investigate  
816 the full set of equations (11), with a particular focus on the question why the whole bacterial  
817 population goes extinct. As it turns out, this requires using finite values for the recovery rate  $\rho$   
818 (instead of the  $\rho \rightarrow \infty$  approximation employed previously).

819 A major difficulty in analyzing the full model (11) is finding appropriate parameter values. In  
820 particular, we need values for the adsorption constant  $\delta$ , the recovery rate  $\rho$  and the yield coefficient  
821  $Y$ . Undiluted LB medium is known to support a population of  $5 \cdot 10^9$  cells/ml. Thus one can easily  
822 estimate  $Y$  as the inverse of this number, when nutrients are measured in units of dilutions, which  
823 we already used throughout this publication (undiluted medium corresponds to  $N = 1$ ). Parameter  
824 scans in simulations reveal that the actual value of the adsorption constant  $\delta$  does usually not  
825 influence the actual outcome (collapsed or surviving bacterial population), it only adjusts time  
826 scales. However, deviations in time scales are insignificant, even when  $\delta$  is changed by orders of  
827 magnitude,  $\delta \sim \mathcal{O}(10^{-6} \dots 10^{-8})$ . They are roughly an hour or less, which is small compared to the  
828 expected duration of the experiment that lasts a few hours. For definiteness, we use the value of  
829  $\delta = 10^{-7} \text{ h}^{-1}$  for our simulations. That the value of the adsorption constant has only a minor impact  
830 on phage growth on bacterial cultures, is also in line with previous findings *Mitarai et al. (2016)*.

831 The most elusive parameter is the recovery rate  $\rho$ . A first indication of the value of  $\rho$  can be  
832 drawn from our experiments on bursting resistant cells, summarized in Fig 2. As the probability  
833 for bursting resistant cells is 3 orders of magnitude smaller than for susceptible bacteria, we can  
834 use  $1/\lambda \sim \mathcal{O}(1)$  to estimate  $\rho \sim \mathcal{O}(10^3)$ . However, our results also indicate that recovery via the  
835 CRISPR/Cas system heavily depends on MOI, implying that  $\rho$  depends on the actual densities of  
836 phages and bacteria. Nevertheless, as experimental determination of recovery is complicated, even  
837 more so determining a functional dependence on dynamically changing densities  $B$  and  $P$ , we  
838 assume that  $\rho$  is constant.

839 We ran parameter sweeps in simulations and compared the outcome – collapsed or surviving  
840 bacterial populations – to the observed experimental results (see Fig 3). The best agreement  
841 of simulations and experiments was reached with  $\rho \sim \mathcal{O}(1)$ . Lower values of  $\rho$  do not allow the



**Appendix 0 Figure 9. Simulated trajectories for all populations in liquid culture for the extended model, including infected and recovering bacteria.** Trajectories are obtained by numerically integrating equations (11), using parameters listed in Table 3 and additionally  $N = 1$ ,  $Y = 2 \cdot 10^{-10} \text{ cells}^{-1}$ ,  $\delta = 10^{-7} \text{ h}^{-1}$  and  $\rho = 1.5 \text{ h}^{-1}$ . (A) For population compositions with a large majority of resistant cells ( $S = 10^{-3}$ ), phages get wiped out fast. (B) For intermediate  $S$  (close to parameters where we observe both, collapsed and surviving, populations, see Fig 3), the populations exhibit a complex, non-monotonic trajectory. After fast initial growth of phages, bacterial populations decay but ultimately can recover. (C) If the fraction of susceptibles is too large ( $S = 0.06$ ), the whole bacterial population is infected and succumbs to the overwhelming phage infection. See supporting text for more detailed information.

842 resistant population to recover from phage infection, while for larger values of  $\rho$ , phages are drained  
 843 from the culture very fast. Such a small value of  $\rho$  is most likely related to the recovery at very large  
 844 MOI, when the densities involved in the dynamics are large, which dominate the overall observed  
 845 dynamics. At this time phages repeatedly infect the same bacteria and their CRISPR/Cas immune  
 846 system cannot deal with such an infection load (or only too slow). Thus, we can argue that our final  
 847 choice  $\rho = 1.5 \text{ h}^{-1}$  is the recovery rate when the CRISPR/Cas system is heavily stressed, which is  
 848 comparable to the actual burst rate  $1/\lambda$  for phages.

849 In Fig 9 we show three exemplary sets of trajectories for bacteria and phage. For a tiny fraction  
 850 of susceptibles,  $S = 10^{-3}$ , which is well below the herd immunity threshold (see Fig 3), phages do  
 851 not thrive on the limited number of favorable hosts and decay fast after a slight increase initially.  
 852 For intermediate fractions of susceptibles,  $S = 0.04$ , we observe more complex, non-monotonic  
 853 trajectories of bacterial populations. For such values of  $S$  we also observe mixed outcomes in  
 854 experiments, see Fig 3. When  $S$  is increased further ( $S = 0.06$ ), enough susceptible bacteria exists  
 855 to produce enough phages and ultimately the whole bacterial population goes extinct.

856 The purpose of the extended model in this section was to justify the fact that phages can wipe  
 857 out the whole bacterial population, which was not possible in the simplified model used in the main  
 858 text. There, the resistant bacterial population was basically unaffected by phages and just acted as

Parameter		Value	Units	Comment
Bacterial growth rate	$a$	0.63	$1/h$	Table 1, Fig 6
Yield	$Y$	$2 \cdot 10^{-1}$	$1/\text{cell}$	Measured in dilution of LB
Recovery rate	$\rho$	1.5	$1/h$	See this appendix
Adsorption constant	$\delta$	$10^{-7}$	$1/(h \text{ cell})$	See this appendix
Diffusion constant	$D$	$1.17 \cdot 10^{-2}$	$\text{mm}^2/h$	See Methods
Burst size	$\beta$	85.6	phages/cell	Table 2, Fig 4
Latency time	$\lambda$	0.60	$h$	Table 2, Fig 4
Initial bacterial population	$B_0$	$10^5$	cells	
Initial phage population	$P_0$	10	phages	

**Appendix 0 Table 3. Parameters used in simulations shown in Fig 9.**



859 “sink” for phages. However, also in this extended model, we see a very similar behavior in terms of  
 860 the threshold phenomena reported earlier in the manuscript.

### 861 **Infection load and efficiency of the CRISPR/Cas system**

862 In the section *Modelling* we showed that positive phage growth leads eventually to a very fast  
 863 increase in the phage population, that occurs before nutrients are depleted (for almost all realistic  
 864 parameters). This behavior of the dynamics was also observed in the extended simulation model  
 865 presented in the last section. Moreover, as a condition we used that the phage population reaches  
 866 a size  $P \sim 1/\delta$ , which is after all arbitrary – it only determines if we can employ useful simplifications  
 867 and approximations to model equations. However, simulation results presented in the last section  
 868 indicate that the bacterial population starts to decay soon after such a threshold  $P \sim 1/\delta$  is  
 869 exceeded.

870 In order to proceed, we investigate the system at time  $T_\delta$  further. We assume that the phage  
 871 population is large enough that it will not be degraded by the CRISPR/Cas immune system. The  
 872 threat to immediate phage extinction is low at this point. The actual equations are hard to solve  
 873 directly, hence we revert to simple balance equations, ignoring the dynamical component. Specif-  
 874 ically, we compare the number of (present and eventually produced) phages to the number of  
 875 infections needed to wipe out the whole population. To incorporate the effects of the bacterial  
 876 immune system in resistant bacteria, we assume that they need  $M > 1$  infections before they burst  
 877 and produce only  $\kappa\beta$  phages, which reduces the burst size by a (yet unspecified) factor  $0 < \kappa < 1$ .  
 878  $\kappa = 1$  implies that resistant cells produce the same number of phages as susceptible cells, while  
 879  $\kappa = 0$  indicates only cell death. Combining these considerations yields

$$\underbrace{1/\delta}_{\text{phages present}} + \underbrace{\beta S_0 B(T_\delta)}_{\text{phage production } B_s} + \underbrace{\kappa\beta(1 - S_0)B(T_\delta)}_{\text{phage production } B_r} > \underbrace{S_0 B(T_\delta)}_{\text{infections } B_s} + \underbrace{M(1 - S_0)B(T_\delta)}_{\text{infections } B_r}, \quad (28)$$

880 where the left side indicates the total number of phages, while the right side indicates the number of  
 881 necessary infections to kill all bacteria. The number of bacteria  $B(T_\delta)$  can be estimated by inserting  
 882 the time  $T_\delta$  from (17) into the exponential growth (14b). Subsequently, we can rearrange (28),  
 883 obtaining a bound on  $M$ :

$$M < \frac{1/\delta B(T_\delta) + S_0(\beta - 1)}{1 - S_0} + \kappa\beta. \quad (29)$$

884 The first term  $1/\delta B(T_\delta)$  indicates the ratio of phages to bacteria at time  $T_\delta$ , and can be considered  
 885 small for non-extremal parameters compared to the other terms. This fact justifies our assumption  
 886 that the actual value of  $\delta$  is not crucial. This number  $M$  might allow some insight into the effective-  
 887 ness of the CRISPR/Cas immune system. For a fraction of susceptibles  $S = 0.03$ , which corresponds  
 888 to the minimal value where we observe only collapsed bacterial populations in undiluted LB medium  
 889 (see Figs 3 and 4), we would obtain the relation  $M \lesssim 3 + 86\kappa$ . Thus, each resistant bacterial cell could  
 890 degrade up to  $\mathcal{O}(10^1 \dots 10^2)$  phages before their CRISPR/Cas system cannot cope with the infection  
 891 load anymore.



**Appendix 0 Figure 10. Image of the scanner system.** Photograph of the scanner system used for time-lapse imaging of phage spread in spatially structured bacterial populations. Three scanners (Epson Perfection V600 Photo Scanner) simultaneously scanned 12 plates in total every 20 minutes in 30°C for 48 hours per experiment.

---

892 **Appendix: Additional information on experimental setup**  
893 Our experimental setup for the scanner system is shown in Fig. 10.